Modular Microstructure Profiler Three
MMP3
July 1996 to Present
Data Channel Description

M. C. Gregg
Applied Physics Laboratory
University of Washington

October 30, 2000

Contents

1 Instrument Configuration

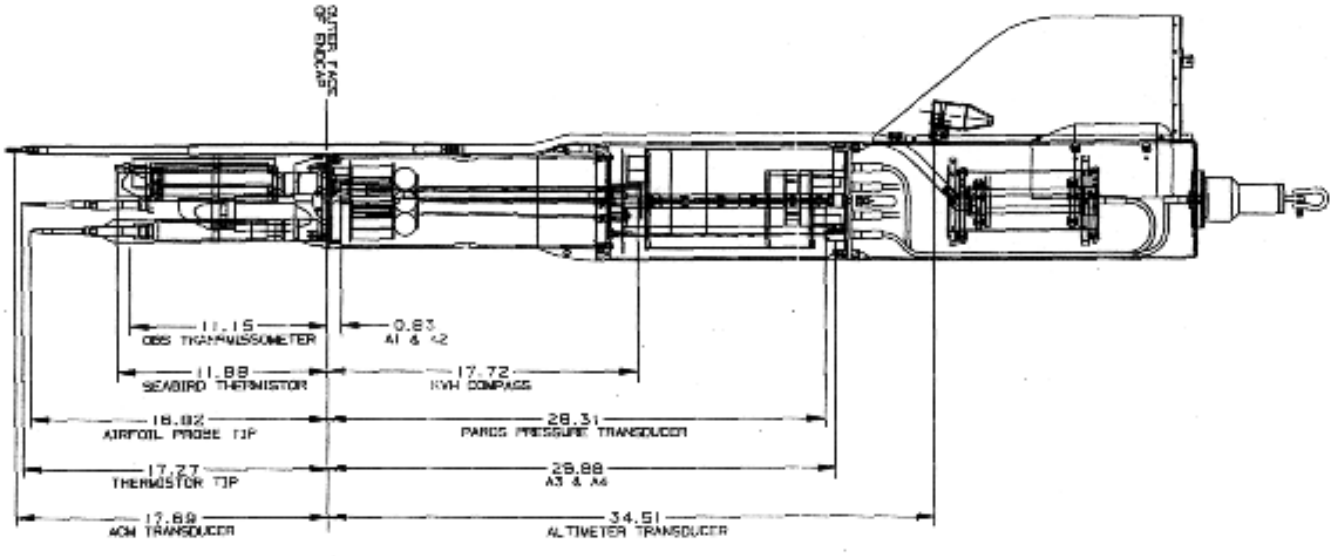

Figure 1: Schematic side view of MMP3 with sensor offsets labeled.

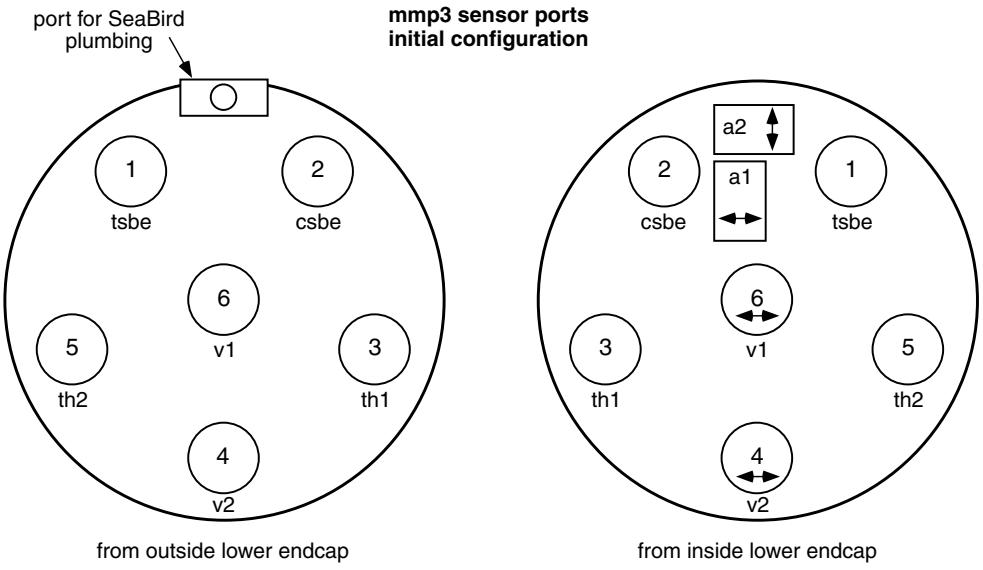

Figure 2: Locations of sensor ports on the lower end cap of mmp3 from July 1996 to the present.

2 Data Channels and Formats

The sensors on MMP3 from July 1996 to the present and their characteristics are given in Table 1.

Variable	Abbr.	Input Range	Output Range	f Hz	Filter Type	Poles	f_{3db} Hz
Acceleration	a1, a2	± 2g max.	±5 V	400	Bessel	4	100
Acceleration	a3, a4	± 2g max.	±5 V	50	Bessel	4	10
Altimeter	ac	$0 - 190$ m	$0 - 32{,}767$ c	25			
Conductivity	c	$0 - 6$ S m^{-1}	$5 - 11$ kHz	25	Hybrid period counter		
Heading	hdg	0^o-359.9^o	0-3599 c	8.33	-	-	-
Optical Back Scatter	obs		$0 - 5$ V	400	Bessel	4	100
Magnetometer	mx,my,mz			25			
Pressure	p	$0 - 6.2$ MPa	$30 - 40$ kHz	25	Hybrid period counter		
Pgauge Temp.	prt	$0°C - 30°C$	$1.375 - 2.050$ V	25			
Relative Velocity	vac1,vac2	± 64.1 cm s^{-1}	±5 V	50	Tch	4	10
Temperature	tl1, tl2		±5 V	400	Bessel	4	100
Temperature	t	$-2°C - 32°C$	$6 - 12$ kHz	25	Hybrid period counter		
Temp. Grad.	th1, th2		±5 V	400	Bessel	4	100
Velocity Grad.	v1, v2		±5 V	400	Tch	6	150

Table 1: MMP3 data channels. Channel tl uses the same thermistor as th1. f_{3db} is the frequency of the anti-alias filter on the channel. The altimeter output is in integral counts.

Anti-alias filters are inside the main electronics case and are wired to the sensor ports.

Some sensors are sampled at 400 Hz and others at 25 Hz, but all are converted to 16-bit digital words. The data are grouped into scans containing 160 words, or 320 bytes (Table 2).

Table 2 shows the scan configuration by sensor port, and Table 3 gives the corresponding set of data channels.

Channels 0 and 1 of each scan are used for the 25 Hz channels. The other channels contain the 400 Hz samples.

The total data rate is

$$10 \text{ channels } \times \frac{2 \text{ bytes}}{\text{word}} \times \frac{400 \text{ samples}}{\text{sec}} = \frac{8,000 \text{ bytes}}{\text{sec}} = \frac{64 \text{ kbits}}{\text{sec}} \; . \qquad (1)$$

The largest data record is likely to be one made to 300 m (MMP's maximum depth) at a fall rate of 0.5 m s^{-1}. It would contain 4.8 Mbytes.

	Column									
Row	1	2	3	4	5	6	7	8	9	10
1	sc	id	tl2	sp3	sp5	sp6	sp4	a1	a2	tl1
2	sp1	sp1	tl2	sp3	sp5	sp6	sp4	a1	a2	tl1
3	sp2	sp2	tl2	sp3	sp5	sp6	sp4	a1	a2	tl1
4	pr0	pr1	tl2	sp3	sp5	sp6	sp4	a1	a2	tl1
5	ac	vb	tl2	sp3	sp5	sp6	sp4	a1	a2	tl1
6	prt	hdg	tl2	sp3	sp5	sp6	sp4	a1	a2	tl1
7	a3	a4	tl2	sp3	sp5	sp6	sp4	a1	a2	tl1
8	vac1	vac2	tl2	sp3	sp5	sp6	sp4	a1	a2	tl1
9	sg	sg	tl2	sp3	sp5	sp6	sp4	a1	a2	tl1
10	sg	sg	tl2	sp3	sp5	sp6	sp4	a1	a2	tl1
11	sg	sg	tl2	sp3	sp5	sp6	sp4	a1	a2	tl1
12	sg	sg	tl2	sp3	sp5	sp6	sp4	a1	a2	tl1
13	sg	mx	tl2	sp3	sp5	sp6	sp4	a1	a2	tl1
14	my	mz	tl2	sp3	sp5	sp6	sp4	a1	a2	tl1
15	a3	a4	tl2	sp3	sp5	sp6	sp4	a1	a2	tl1
16	vac1	vac2	tl2	sp3	sp5	sp6	sp4	a1	a2	tl1

Table 2: MMP3 sensor ports betweenJune 1999 and the present. The sensor ports are designated as sp1 to sp6, and their locations are shown in Fig. 1. Other symbols are: sc for scan count, id for mmp vehicle number, al is for the altimeter, vb for battery voltage, and sg for signal ground. Blank positions are also at signal ground. Each position corresponds to 2 of the 320 bytes in a scan.

There are 25 scans per second.

	Column									
Row	1	2	3	4	5	6	7	8	9	10
1	sc	id	tl2	th1	obs or th2	v1	v2	a1	a2	tl1
2	t0	t1	tl2	th1	obs or th2	v1	v2	a1	a2	tl1
3	c0	c1	tl2	th1	obs or th2	v1	v2	a1	a2	tl1
4	pr0	pr1	tl2	th1	obs or th2	v1	v2	a1	a2	tl1
5	ac	vb	tl2	th1	obs or th2	v1	v2	a1	a2	tl1
6	prt	hdg	tl2	th1	obs or th2	v1	v2	a1	a2	tl1
7	a3	a4	tl2	th1	obs or th2	v1	v2	a1	a2	tl1
8	vac1	vac2	tl2	th1	obs or th2	v1	v2	a1	a2	tl1
9	sg	sg	tl2	th1	obs or th2	v1	v2	a1	a2	tl1
10	sg	sg	tl2	th1	obs or th2	v1	v2	a1	a2	tl1
11	sg	sg	tl2	th1	obs or th2	v1	v2	a1	a2	tl1
12	sg	sg	tl2	th1	obs or th2	v1	v2	a1	a2	tl1
13	sg	mx	tl2	th1	obs or th2	v1	v2	a1	a2	tl1
14	my	mz	tl2	th1	obs or th2	v1	v2	a1	a2	tl1
15	a3	a4	tl2	th1	obs or th2	v1	v2	a1	a2	tl1
16	vac1	vac2	tl2	th1	obs or th2	v1	v2	a1	a2	tl1

Table 3: MMP3 data scan format, used from June 1999 to the present. Symbols in addition to the standard channel mnemonics are: sc for scan count, id for mmp vehicle number, t0 and t1 for two halves of wbo temperature word (tsbe), c0 and c1 for two halves of wbo conductivity word (csbe), ac for altimeter, vb for battery voltage, sg for signal ground, and hdg for heading.

3 Analog to Digital Conversion

The analog-to-digital converter is an Analog Devices DAS1159 low-power unit that uses 2's complement coding to convert -5 volts to +4.99985 volts into 16-bit digital words that range from -32,768 to 32,767. Including zero, the output range is 65,536. For a channel with a 10 volt input the least count is

$$V_{\rm lc} = \frac{10 \text{ volts}}{2^{16} - 1 \text{ counts}} = 152.588 \ \frac{\mu\text{V}}{\text{count}}. \tag{2}$$

As seen in Figure 3, observed least count in tl1 matches the expected value. Data are converted from counts to volts by multiplying by (2).

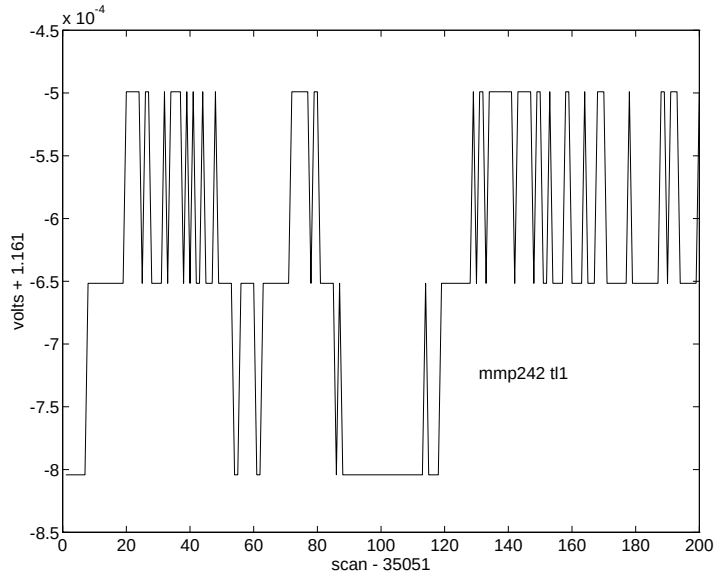

Figure 3: Expanded-scale plot of tl1 showing digital noise.

The variance of the quantization noise spectrum depends on both the amplitude and the correlation structure of the quantization error. If the error is uniformly distributed, i.e. if the spectrum is flat,

$$V^2_{\rm quant} = \frac{{V_{\rm lc}}^2}{12} \quad [\text{V}^2] \ . \tag{3}$$

(Section 3.4 of *Otnes and Enochson* (1978)). The corresponding spectral density is

$$\Phi_{\rm quant}(f) = \frac{V^2_{\rm quant}}{f_{\rm N}} = \frac{{V_{\rm lc}}^2}{12 f_{\rm N}} = 9.85 \times 10^{-12} \quad [\text{V}^2 \ \text{Hz}^{-1}] \ , \tag{4}$$

where $f_{\rm N}$ is the Nyquist frequency. The observed spectrum of tl1 is flat for $F > 30$ Hz, but the amplitude is 2.4×10^{-11} V^2 Hz^{-1} (Fig. 4). Because other channels show similar minimum levels, this appears to be the true quantization spectrum and indicates that the A/D does not produce uncorrelated errors.

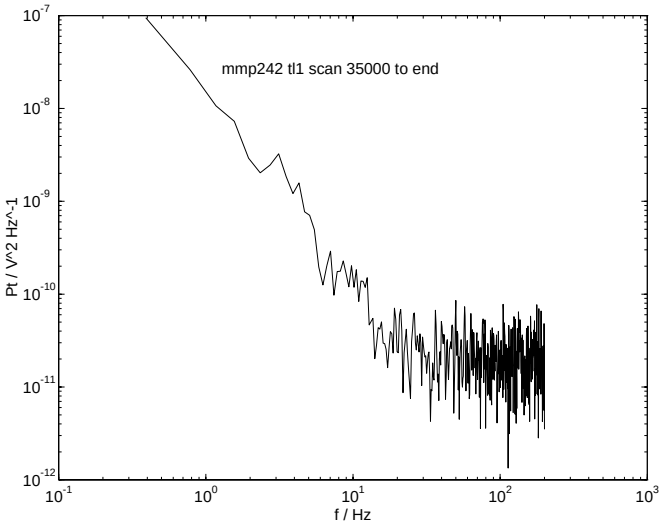

Figure 4: Spectrum of tl1, showing a flat noise spectrum at high frequency.

4 Analog Filters

All of the anti-alias filters are in the main electronics case and are thus tied to sensor ports.

4.1 Bessel Low Pass

Several of the MMP channels (a1, a2, tl1, tl2, th1, th2)use a 4-pole Bessel low-pass filter with 3-db attenuation at $f_c = 100$ Hz. Two accelerometer channels, a3 and a4, use a similar filter except with $f_c = 10$ Hz.

$$H^2_{\text{Bessel4}}(f) = \frac{b_0^2}{(b_0 - b_2(cf)^2 + b_4(cf)^4)^2 + ((b_1 c)f - b_3(cf)^3)^2} \tag{5}$$

$$\phi_{\text{Bessel4}}(f) = \tan^{-1}\left(\frac{-(b_1 cf - b_3(cf)^3)}{b_0 - b_2(cf)^2 + b_4(cf)^4}\right) \tag{6}$$

Parameter values are listed in Table 4.

Parameter	Value
b_0	105
b_1	105
b_2	45
b_3	10
b_4	1
c	2.115 f_{3db}^{-1}
f_c	100 Hz (10 Hz for a3, a4)

Table 4: Parameter values for the 4-pole Bessel low-pass filters used in MMP3. $H^2_{\text{Bessel4}}(f_{3db}) = 0.5$.

The phase shift of a constant time delay, τ, is $\phi(f) = -2\pi f\tau$ [rad].
The amplitude-squared and phase response are plotted in Figure 5.

4.2 Tchhebyschev Low Pass

Outputs from the airfoil and acoustic current meter circuits are fed to Tchebyshev type I lowpass filters to minimize aliasing. These filters produce lobes with equal magnitudes of ripple in the passband and are maximally flat in the stopband. They, however, roll off more rapidly than Chebyshev type II filters, which are maximally flat in the passband and equiripple in the stop band. The MMP3 filters are made by Frequency Devices of Haverhill, MA. The filters have 0.2 db passband ripple and rolloff by 3 db at 100 Hz for the airfoils and 10 Hz for the acoustic current meter.

Filter manuals differ in how they specify f_c, the cutoff frequency, for Tchebysheff filters. Frequency Devices specifies it as $f_c = f_{3db}$, where $db \equiv -10 \log_{10} H^2$. Matlab specifies f_c as

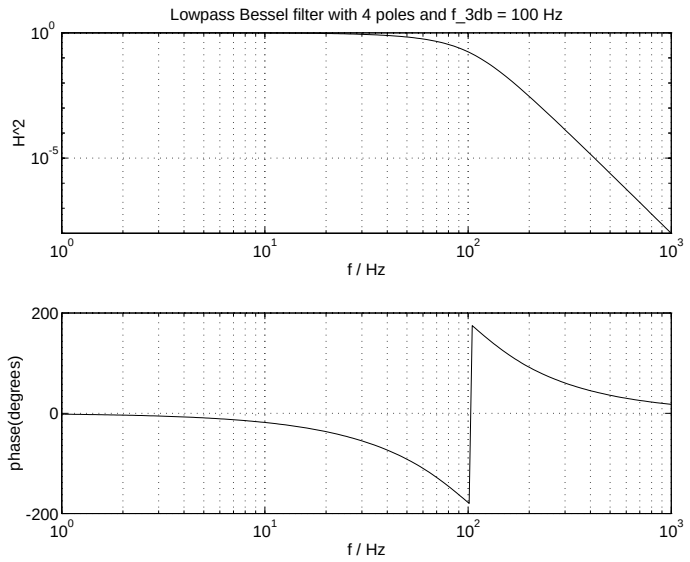

Figure 5: Amplitude-squared and phase response of the 4-pole Bessel low-pass filter with 3-db attenuation at $f_c = 100$ Hz.

the frequency where the rolloff has the same amplitude as the passband ripple. *Williams* (1981) (Section 2.4) gives expressions to reconcile the different cutoff frequencies.

Take R_{db} as the passband ripple in db ($R_{db} = 0.2$ in our case). First calculate

$$\epsilon = \sqrt{10^{R_{db}/10} - 1} \tag{7}$$

and

$$A = \frac{1}{n} \cosh^{-1}(1/\epsilon) \ , \tag{8}$$

where n is the number of poles. Then

$$f_{R_{db}} = \frac{f_{3db}}{\cosh A} \ . \tag{9}$$

For the MMP3 airfoil filters ($R_{db} = 0.2$ and $n = 6$) $\epsilon = 0.2170911$, $A = 0.3681$, and $\cosh A = 1.068517$, giving $f_{R_{db}} = 93.5877$ Hz.

The magnitude-squared response is

$$H^2_{\rm Tch}(f) = \frac{1}{1 + \epsilon^2 C_n^2(\Omega)} \ , \tag{10}$$

where $C_n^2(\Omega)$ is the n-th order Tchebysheff polynomial, and

$$\Omega \equiv \frac{f}{f_{3db}} \cosh A \ . \tag{11}$$

For $n = 6$,

$$C_6^2 = 32\Omega^6 - 48\Omega^4 + 18\Omega^2 - 1 \ . \tag{12}$$

The response was evaluated with Matlab and plotted in Figure 6. Comparison with

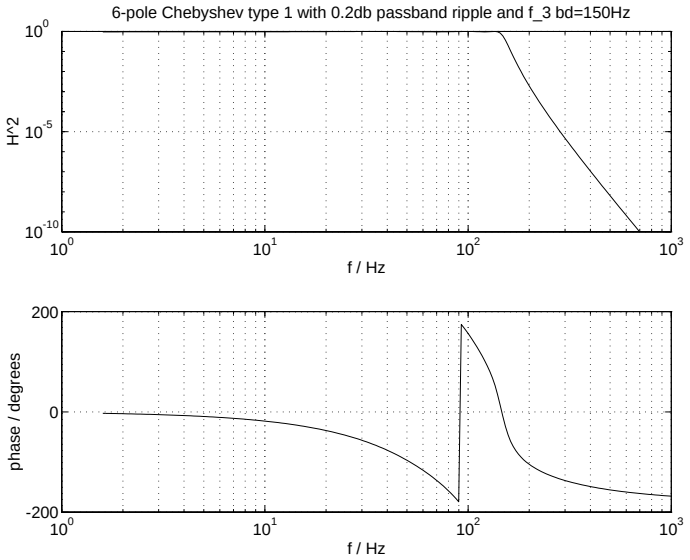

Figure 6: Transfer function of the Tchebyshev lowpass filter used with the MMP airfoil probes.

values given in the Frequency Devices filter handbook agree within about 0.2 db and several tenths of a degree. At the Nyquist frequency, 200 Hz, the magnitude-squared response is about 3×10^{-3}, which may not be enough to prevent detectable aliasing if there are strong vibrations at that or higher frequencies.

To simulate or correct for the magnitude-squared response for the MMP3 airfoil channels use

$$H^2_{\mathrm{Tch6}} = \frac{1}{1 + 0.2171^2 \left(32(f/140.3815)^6 - 48(f/140.3815)^4 + 18(f/140.3815)^2 - 1\right)} \ . \tag{13}$$

ANALYTIC FORM OF PHASE SHIFT.

For the MMP3 acoustic current meter filters (R_{db} = 0.2 and n=4) $\epsilon = 0.2170911$, A = 0.55215 and cosh A = 1.156346, giving $f_{R_{db}}$=8.6479 Hz.

5 Period Counters

Sea-Bird temperature and conductivity sensors produce frequency-modulated signals that are digitized by a hybrid counter developed by Art Pederson and described in the Sea-Bird CTD manual. MMP3 uses the same type of counting scheme, with different IC's, and the same model of reference crystal. The MMP3 crystal is a Vectron model Co-441E-5X with a 8.192 MHz nominal frequency. The unit in MMP3 has been measured at $f_r = 8,192,678$ Hz. Its specifications are an accuracy of ± 1 ppm and stability between 0°C and 50°C of ± 5 ppm. The count is done over the full scan and the time needed determined the low frequency scan rate of 25 Hz.

The crystal sets the timing of both analog-to-digital and period counters. The A/D sample rate is set by counting 20,480 cycles of the reference frequency. The period-counting rate is 1/16 of the A/D sample rate and is set by counting 327,680 reference cycles. Hence, the interval for period counting is

$$\tau_{f_r} = \frac{f_r}{327,680} = 39.996758 \quad [\text{ms}] \ , \tag{14}$$

and the actual sampling frequency is $\tau_{f_r}^{-1} = 25.002026367$ Hz.

Pederson developed the hybrid counter to obtain better frequency resolution than given by simple period counting. Simple period counting would give the sensor frequency as

$$f_s = \frac{N_s}{\tau_{f_r}} \quad [\text{Hz}] \ , \tag{15}$$

where N_s is the number of positive-going zero-crossings of the sensor output during τ_{f_r}. The uncertainty is $df_s = dN_s/\tau_{f_r}$. Consequently, least count in N_s, i.e. $dN_s = \pm 1$ count, corresponds to a frequency uncertainty of $df_s = \pm 25$ Hz. Because the sensor frequencies are 5-12 kHz, this would correspond to fractional errors of ± 0.005 to ± 0.002.

The major uncertainty results from τ_{f_r} not being an integral number of sensor cycles. The hybrid period counter reduces this uncertainty by using two 12-bit counters. One counter, N_s, is incremented by positive-going zero-crossings of the sinusoidal sensor output. The other counter, N_r, is incremented by positive-going edge-crossings of the reference signal, which is a square wave between 0 and +5 volts.

As shown schematically in Figure. 7, N_s is reset just after being incremented by the first zero-crossing in each scan. Consequently, N_s^i is the number of complete sensor cycles between the first zero-crossing in the ith scan and the first zero-crossing in the $i+1$st scan. N_r is reset at the beginning of each scan and stopped when the sensor makes it first zero-crossing of the scan. This occurs $\delta t_{i-1} = N_r^{i-1}/f_r$ seconds after the start of the ith scan and next again at $\delta t_i = N_r^i/f_r$ seconds after the start of the $i+1$th scan. Therefore, the time required for the N_s^i sensor cycles is $\tau_{f_r} + \delta t_i - \delta t_{i-1}$. It follows that the sensor frequency is

$$f_s = \frac{N_s}{\tau_{f_r} + \delta t_i - \delta t_{i-1}} = \frac{N_s^i f_r}{f_r \tau_{f_r} + N_r^i - N_r^{i-1}} = \frac{N_s^i f_r}{327,680 + N_r^i - N_r^{i-1}} \ . \tag{16}$$

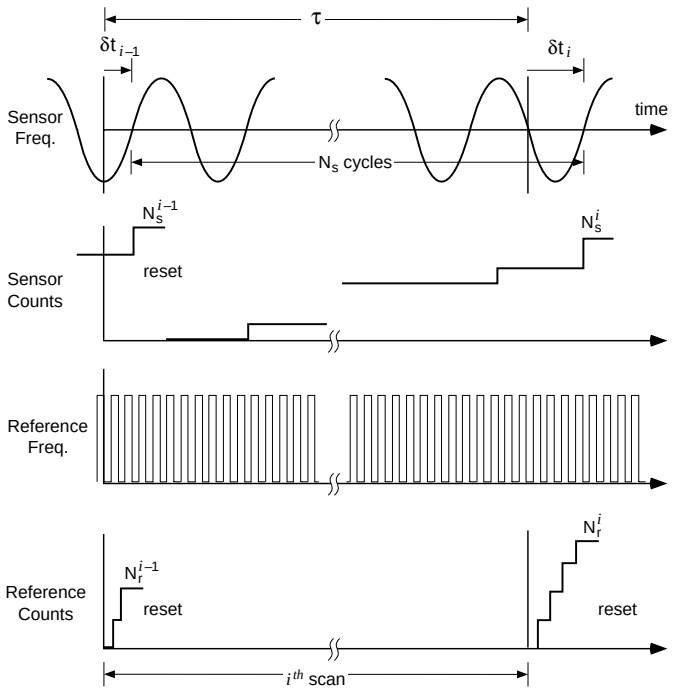

Figure 7: Schematic of period counting. N_s is the number of positive-going zero-crossings of the sensor frequency, f_s. N_r is the number of positive-going edge crossings of the reference frequency, f_r.

The accuracy is limited only by the stability of f_r and the least-count uncertainty in counting it.

Temperature and conductivity are counted in parallel, and their frequencies are averages over the scan. Hence, to be aligned in time with the A/D channels, period counted variables should be shifted to the middle of the previous scan. Each requires 24 bits per scan and thus occupies two adjacent data words. Initially on MMP3 the SeaBird temperature probe is installed in sensor port 1 and the data written in scan words 10 and 11 (where the first word is numbered 0). SeaBird conductivity is installed in sensor port 2 and the data written in words 20 and 21 (Tbl 3). Their packing is shown in Table 5.

Channel 0		Channel 1	
ms byte	ls byte	ms byte	ls byte
$s_{11}s_{10}s_9s_8s_7s_6s_5s_4$	$s_3s_2s_1s_0r_{11}r_{10}r_9r_8$	$r_7r_6r_5r_4r_3r_2r_1r_0$	00000000

Table 5: Packing format for $t0$ and $t1$ and for $c0$ and $c1$, the Sea-Bird temperature and conductivity data. s_{11} and r_{11} are the most significant bits of the sensor and reference count, and s_0 and r_0 are the least significant bits.

Because the final count is a difference from the previous count, the first words in a file are always bad and should be discarded.

5.0.1 Least Count

The uncertainty in sensor frequency, df_s results from least count errors in N_s^i, N_r^i and N_r^{i-1}. This can be estimated by differencing (16) to obtain

$$df_s^i = \frac{f_r^i}{327,680 + N_r^i - N_r^{i-1}} dN_s^i - \frac{N_s^i f_r^i}{(327,680 + N_r^i - N_r^{i-1})^2}(dN_r^i - dN_r^{i-1}) \quad \text{[Hz]} \; . \tag{17}$$

Assuming that the least-count errors are uncorrelated, the frequency variance due to least count is $(df_s^i)^2 = a_1(dN_s^i)^2 + a_2(dN_r^i)^2 + a_3(dN_r^{i-1})^2$. Because $N_r^i - N_r^{i-1}$ is much smaller than 327,680, this can be simplified to

$$(df_s^i)^2 \approx 25^2(dN_s^i)^2 - 0.313 \times 2 \times (dN_r^{i-1})^2 \; . \tag{18}$$

5.0.2 Accuracy

Again, following the Sea-Bird CTD manual, temperature sensitivity of f_r affects the accuracy of the counts.

6 Altimeter, ac

To obtain the height of MMP3 above the bottom when profiling in shallow water, we use a small acoustic transducer. The transducer has been mounted on one of the fins, but that position is more likely to disturb the flow. Consequently, the transducer is usually mounted on the tube.

Each pulse contains 75 cycles of 368,640 Hz sound and nominally lasts 200 μsec. Hence, pulses are about 0.3 m long in water.

The transducer can be pulsed at rates of 1.25, 2.5, and 5 Hz. With the present rate of 25 scans per second, these rates correspond a pulse every 20, 10, and 5 scans. Pulsing at 5 Hz and using fall rates of $w = 0.6$–0.8 m s^{-1} results in a pulse being transmitted every 0.12–0.16 m along the vehicle's vertical path.

If the altimeter is at height h_0 when pulsed, the distance traveled by the pulse between transmission and reception is

$$c\Delta t_{\text{in water}} = \frac{h_0}{\cos\theta_{\text{ac}}} + \frac{h_0 - w\Delta t_{\text{in water}}}{\cos\theta_{\text{ac}}} \ , \tag{19}$$

where c is the average sound speed and θ_{ac} is the inclination of the altimeter to the axis of the MMP tube. Typically, $\theta_{\text{ac}} \approx 5°$. The maximum range of the altimeter is about $h_0 = 50$ m giving $\Delta t_{\text{in water}} \approx 67$ ms. Solving for the height,

$$h_0 = \frac{\Delta t_{\text{in water}}(c\cos\theta_{\text{ac}} + w)}{2} \ . \tag{20}$$

In addition to $\Delta t_{\text{in water}}$, the measured time interval between transmission and reception, Δt, includes a phase delay in the electronics,

$$\Delta t = \Delta t_{\text{in water}} + \Delta t_{\text{electronics}} \ . \tag{21}$$

Measurements with an oscilloscope show $\Delta t_{\text{electronics}} \approx 0.1$ ms and would produce an error of about 75 mm if the delay is not subtracted from the measured time.

If measured sound speed is not available, it can be computed using

$$c = 1449.2 + 4.623T - 0.0546T^2 \quad [\text{m s}^{-1}] \tag{22}$$

The transducer is electronically blanked for 1.5 ms after being pulsed. Consequently, no return can be received when the bottom is closer than 1.125 m to the altimeter face.

Depending on where data recording begins relative to the scan cycle, the first pulse in a particular record will be transmitted between scans 1 and 5. The altimeter pulse is keyed to the position of the altimeter word in a data scan, as shown in Figure 8.

Travel times are written as 16 bit words and can vary from 0 to $2^{15}/128,000$ s$^{-1} = 0.256$ s. When no echo is detected, the most significant bit is set to 1 and the lower bits are set to 0 giving the count as $-2^{15} = -32,768$.

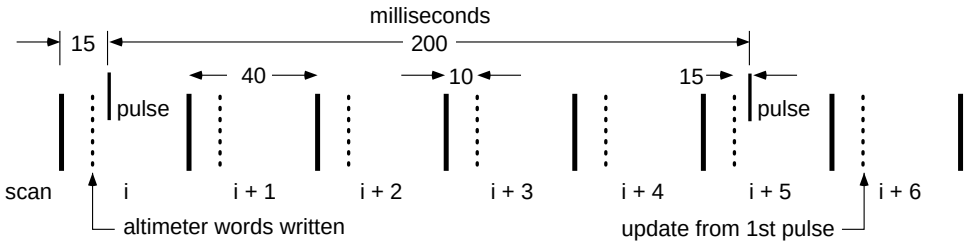

Figure 8: Altimeter timing. Because 25 scans are written per second, scans begin at intervals of 40 ms. With the present scan configuration, the altimeter word is written 10 ms after the start of the scan, and the altimeter is pulsed 5 ms after that. The altimeter word is updated every 5 scans, but an additional scan is needed to insert the new count into the data stream. Consequently, height is updated 6 scans after the pulse is transmitted.

The counts give the number of clock cycles elapsed after a pulse is transmitted. Because the clock frequency is 128 kHz the elapsed time is

$$\Delta t = \frac{\text{counts}}{128,000} \ . \tag{23}$$

The minimum time increment corresponding to the least digital count is

$$dt = \frac{1}{128,000 \ \text{s}^{-1}} = 7.81 \ \mu\text{s} \ . \tag{24}$$

The corresponding resolution in height (half of round-trip distance) is

$$dz = \frac{7.81 \ \mu\text{s} \times 1500 \ \text{m s}^{-1}}{2} = 5.86 \ \text{mm} \ . \tag{25}$$

7 Battery Voltage, vb, and Signal Ground, sg

7.1 Battery Voltage, vg

Approximatedly one-fourth the battery voltage is sampled in counts in vb. To get the voltage in volts, use vb [V]= $152.588\times10^{-6}/0.249$ vb [counts]. (Fig. 9).

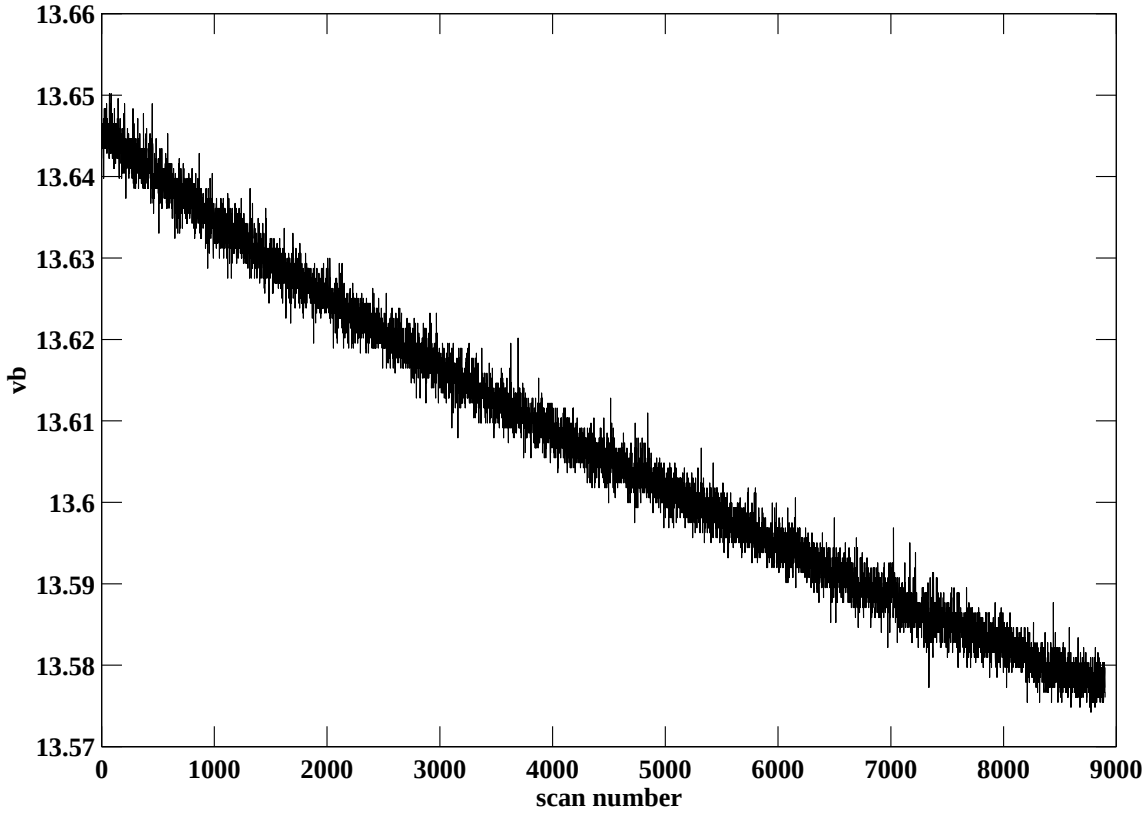

Figure 9: Example of data from the vb channel.

7.2 Signal Ground, sg

Signal ground, sg, is plotted in Figure 10. sg [V] = 152.588×10^{-6} sg [counts]

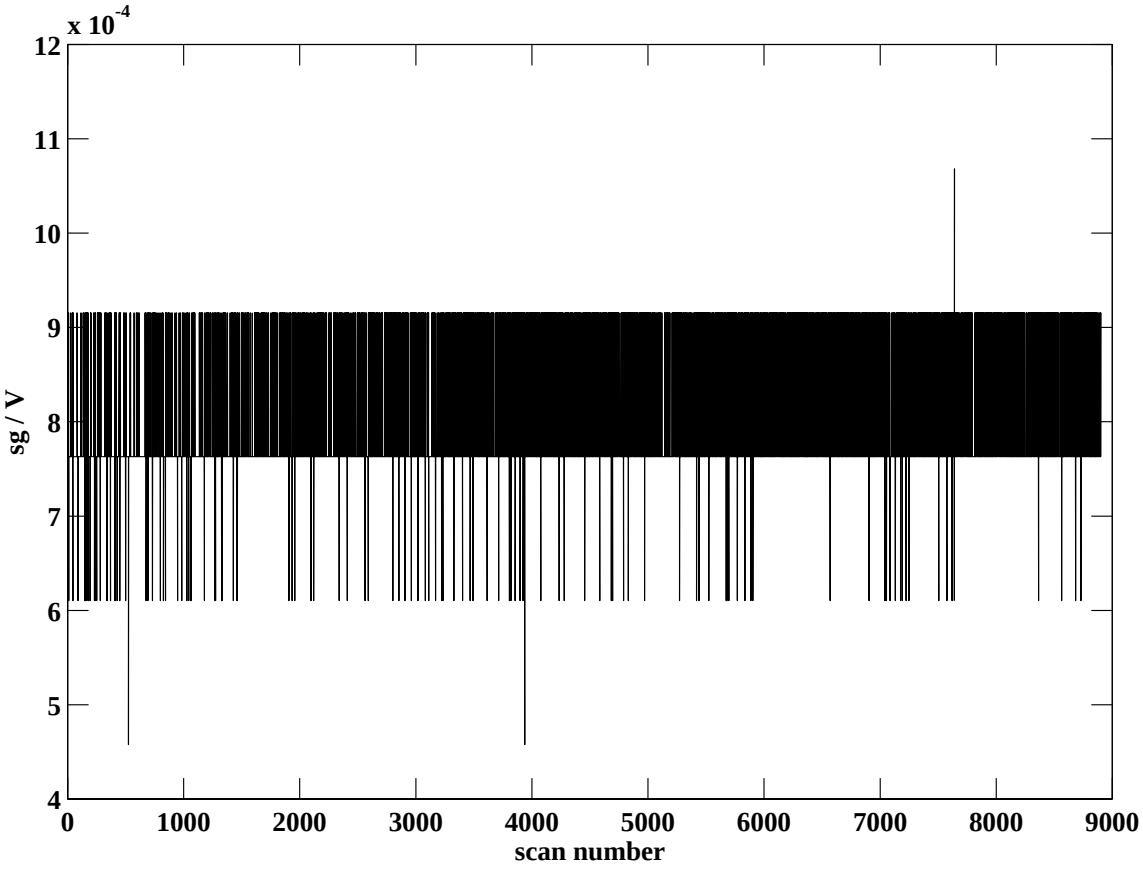

Figure 10: Example of data from the sg channel.

8 Acceleration, a1, a2, a3 and a4

8.1 Sensor Characteristics

MMP3 contains four accelerometers, two aligned with the x-axis and two with the y-axis. One x-y pair, a1 and a2 respectively, is mounted on the lower end cap while the other x-y pair, a3 and a4, is mounted on the top end cap just below the flooded section. The a1 and a3 accelerometers are aligned so their sensitive axis is parallel to the sensitive axis of airfoil v2. The accelerometers are used to measure vehicle tilt and have a gain of 21. The two pairs are separated by 74.7 cm.

The accelerometers are Model 3140 by KSensors of Milpitas, CA. For a standard input range of ±2 g their output range is ±2 volts. The manufacturer states that the sensors can withstand accelerations 20 times the rated range.

Sensitivity, S_a, of these units is nominally 1 volt per g or

$$S_a = \frac{1 \text{ volt}}{9.8 \text{ m s}^{-2}} = 0.102 \frac{\text{V}}{\text{m s}^{-2}} \ . \tag{26}$$

Consequently, the output voltage from a sensor is

$$V = \frac{aS_a}{g} + V_0 \ , \tag{27}$$

where a is the acceleration, and V_0 the output when the mmp is vertical and not accelerated horizontally.

As shown in Figure 11, tilts of θ_x and θ_y from vertical produce accelerations of

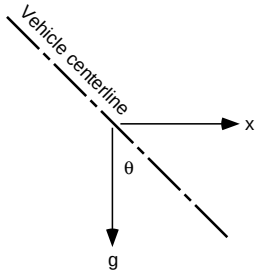

Figure 11: Horizontal acceleration produced by instrument tilt.

$$\frac{d^2x}{dt^2} = -g \sin\theta_x \quad \text{and} \quad \frac{d^2y}{dt^2} = -g \sin\theta_y \ . \tag{28}$$

The sign of the tilt for a1, a2, a3, a4 on MMP3 is determined as follows: on MMP3 the x-axis is a line running through ACM transducers x1 and x2. Positive x is a tilt of the nose in the direction of x1 (towards port 3 on MMP 1 and 2). The sign of a1 for such a tilt is positive while the sign for a3 is negative.

On MMP3 the y-axis is a line running through the ACM transducers y1 and y2. Positive y is a tilt of the nose in the direction of y2 (towards the conductivity ducting between port 1 and 2 on MMP 1 and 2). The sign of a2 for such a tilt is positive while the sign for a4 is negative.

The sensor has unity response, with ±5%, from 0 Hz to 250 Hz and an output of +2.493 volts for a steady zero input. Typical sensitivity to transverse accelerations is stated to be ±1.0% of the full-scale span, or ±0.098 m s^{-2}. Maximum transverse sensitivities are given as three times larger.

Typical accuracy is stated to be ±0.2% of the signal span, or $\pm 1.96 \times 10^{-2}$ m s^{-2}. The worst case is stated as ±1.0% of the signal span or ±0.098 m s^{-2}.

Typical temperature coefficients of the sensitivity are ±1% of full-scale for a temperature range of -20°C to +85°C. Worst cases are twice as large. These correspond to $\pm 9.3 \times 10^{-4}$ m s^{-2} to $\pm 1.9 \times 10^{-3}$ m s^{-2}. The temperature coefficient of the zero output is given as the same.

Output noise is specified as 0.5 mV peak-to-peak.

8.2 Electronics

In the MMP3 circuit (Fig. 12), the accelerometer output is fed to the positive input of a

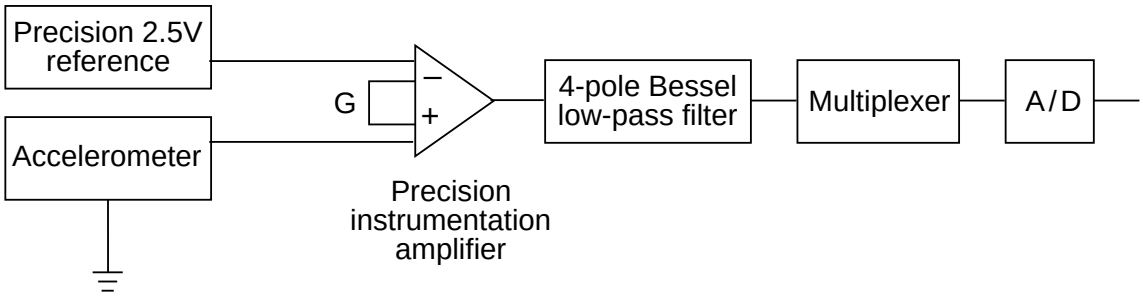

Figure 12: Schematic of the accelerometer circuit.

precision instrumentation amplifier, and a precision 2.5 v reference is fed to the negative input. This retains the dc sensitivity and gives zero output when the instrument is vertical. The amplifier gain is $G_{ac} = 21$. Therefore, the output is

$$V = 21 S_a \frac{d^2x}{dt^2} + V_0 \quad [\text{m s}^{-2}] \,, \tag{29}$$

where a is the input acceleration, and V_0 is the output when the instrument is vertical. Until we determine otherwise, we will use $V_0 = 0$.

The four-pole Bessel filters used for a1 and a2 are down 3 db at 100 Hz. The four-pole Bessel filters used for a3 and a4 are down 3 db at 10 Hz.

8.3 Data Conversion

To compute acceleration,

$$\frac{d^2x}{dt^2} = \frac{g}{S_a G_{ac}}(V - V_0) \quad [\text{m s}^{-2}] \ . \tag{30}$$

To compute the tilt angle

$$\theta_a = \sin^{-1}\left(\frac{V}{g21S_a}\right) \ . \tag{31}$$

Outputs of ± 5 V correspond to $\theta_a = \pm\sin^{-1}(5/(g21S_a))$ or $\pm 13.8°$.

8.3.1 Scaling Spectra

The spectrum of output data expressed in volts is

$$\Phi_{\rm R}(f) = \Phi_a(f) S_a^2 10^4 \Phi_{\rm Bessel4}(f) \quad [\text{Volts}^2\ \text{Hz}^{-1}] \ , \tag{32}$$

where $\Phi_a(f)$ is the spectrum of horizontal acceleration as a function of frequency. It follows that

$$\Phi_a(f) = \frac{\Phi_{\rm R}(f)}{S_a^2 10^4 \Phi_{\rm Bessel4}(f)} \quad [(\text{m s}^{-2})^2\ \text{Hz}^{-1}] \ . \tag{33}$$

This can be converted to a spectrum of horizontal velocity with

$$\Phi_u(k_3) = \frac{\Phi_a(k_3)}{(2\pi f)^2} \quad [(\text{m/s})^2\ \text{cpm}^{-1}] \ . \tag{34}$$

The wavenumber spectrum of horizontal acceleration is given by

$$\Phi_a(k_3) = \frac{w\Phi_{\rm R}(f)}{S_a^2 10^4 \Phi_{\rm Bessel4}(f)} \quad [(\text{m s}^{-2})^2\ \text{cpm}^{-1}] \tag{35}$$

Dividing by $(2\pi k_3)^2$ converts this to velocity as a function of vertical wavenumber. Direct comparison with airfoil data requires knowing the nature of the motion. Vibrations likely form standing waves and differ in amplitude with position. Hence, the accelerometer may not be a good measure of vibration at the airfoils. If the tube is tilting, velocity at the airfoils depends on the distance between the center of buoyancy and the airfoils.

Tilts produce signals of the same sign in the upper and lower accelerometers. Angular accelerations produce signals of opposite sign. Averaging the two removes the latter contributions to the accelerometer records, making more reliable tilt estimates than using a1 or a3 alone.

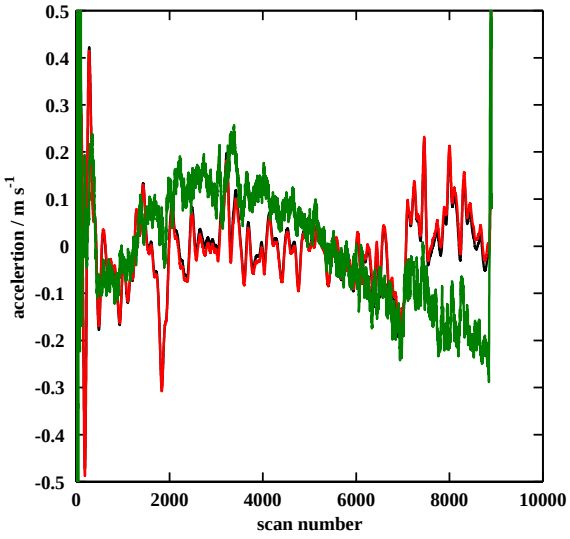

Figure 13: A typical record of a1 (black), a3 (red), and ten times their difference (green).

8.4 Observed Characteristics

Typical records of a1 (black), a3 (red) and ten times their difference (green) are plotted in figure 13. The difference is due to angular acceleration at higher frequencies, and may be due to temperature-dependendent offsets at low frequency.

Power spectra of raw accelerometer records are dominated by large peaks at frequencies near 20 Hz and higher (Fig.). These levels obscure the accelerometer noise,

$$\Phi_{\rm R}^{\rm noise}(f) = \frac{10^4 5 \times 10^{-4\,2}}{(6.6)(200)} = \frac{1.25 \times 10^{-5}}{6.6} \quad [\text{Volts}^2\ \text{Hz}^{-1}]\ , \tag{36}$$

where 6.6 is the rule-of-thumb relation between peak-to-peak and rms noise. A pk-pk value of 6.6 x V_{RMS} occurs no more than 0.1% pf the time (Gaussian noise distribution). The noise voltage will exceed a pk-pk value of 2 x V_{RMS} for 32% of the time. After conversion to acceleration units the previous spectrum is shown in Figure. In section 17 the velocity signature of the acceleration signals is examined.

Spectra of a1, a3 and their difference and mean are shown in figure 14.

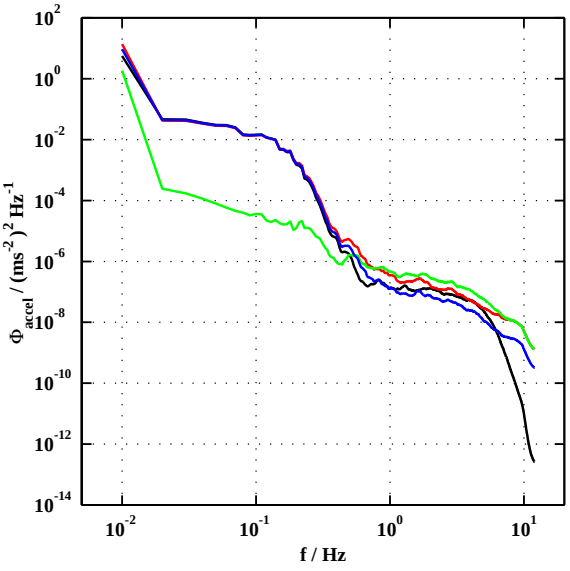

Figure 14: Spectra of a1 (black), a3 (red), their difference (green), and their mean (blue).

9 Conductivity (Sea-Bird), c

9.1 Sensor Description

The sensor is a Sea Bird Model SBE-4 conductivity meter. Water is pumped through the cell using a Sea-Bird pump that has nominal flow rates of 28 ml/s when the pump runs at 3000 rpm and 43 ml/s when the pump is set for 4500 rpm. The cell has three electrodes (Fig. 15). The outer electrodes are connected electrically and thus are in parallel. Their combined resistance is one leg of a Wien bridge oscillator circuit. Full scale is usually 1.4 S m^{-1} to 5.8 S m^{-1}, and produces oscillator frequencies of 5 kHz to 11 kHz.

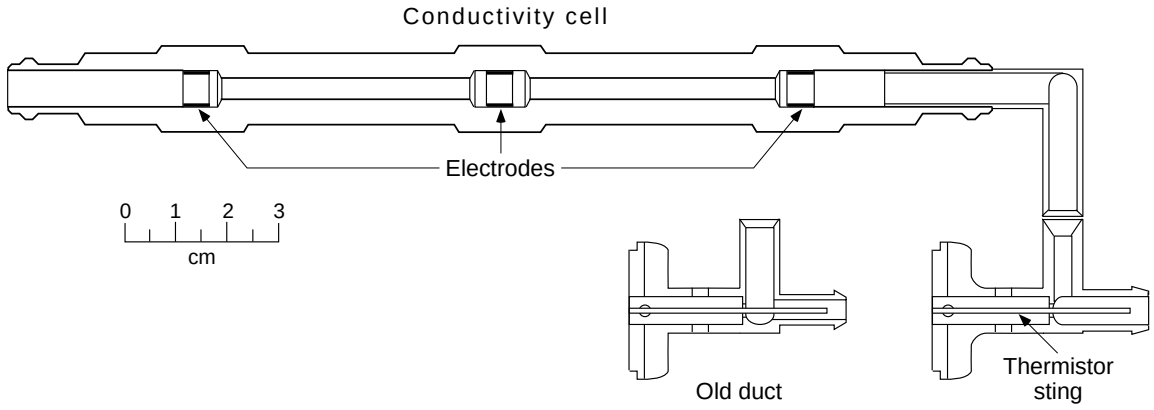

Figure 15: Schematic of ducted Sea-Bird conductivity cell with temperature probe.

9.1.1 Static Response

Calibrations are fitted with

$$c = \frac{af^m + bf^2 + c + dT}{10(1 - 9.57 \times 10^{-6} p)} \quad [\text{S m}^{-1}\ ]\ , \tag{37}$$

where T is the in-situ temperature, f is the probe frequency in kHz, and p is in-situ pressure in MPa. (Note: Sea-Bird expresses pressures in db and uses a coefficient of 10^{-8} for the pressure correction.) The calibration of probe 1170 on 7 April 1994 gives $a = 1.18828817 \times 10^{-3}$, $b = 5.38355432 \times 10^{-1}$, $c = -4.13529688 \times 10^{0}$, $d = -9.89470584 \times 10^{-4}$, and $m = 2.8$. Residuals from the fit vary from -0.14 mS/m to 0.23 mS/m. Equation 37 evaluated with these coefficients is plotted in Figure 16.

Numerically differentiating (37) gives the sensitivity, df/dc, shown in Figure 17. It decreases markedly with increasing conductivity.

9.1.2 Data Conversion

The sinusoidal output is counted as described in Section 5.

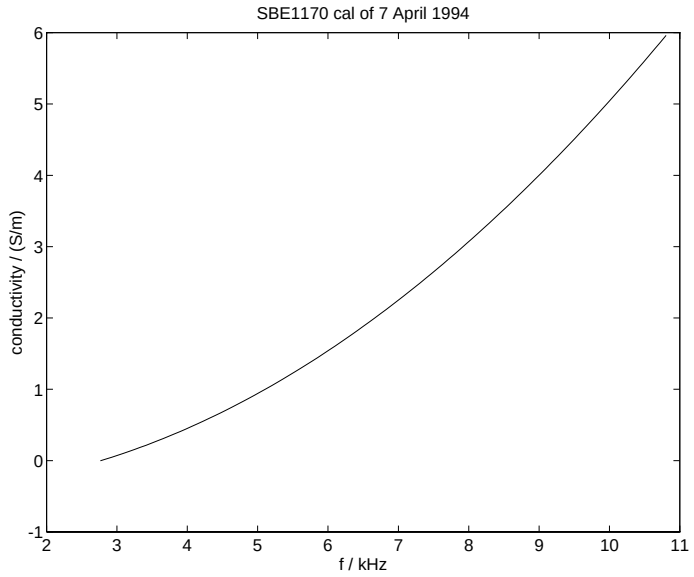

Figure 16: Conductivity as a function of frequency for the Sea-Bird cell.

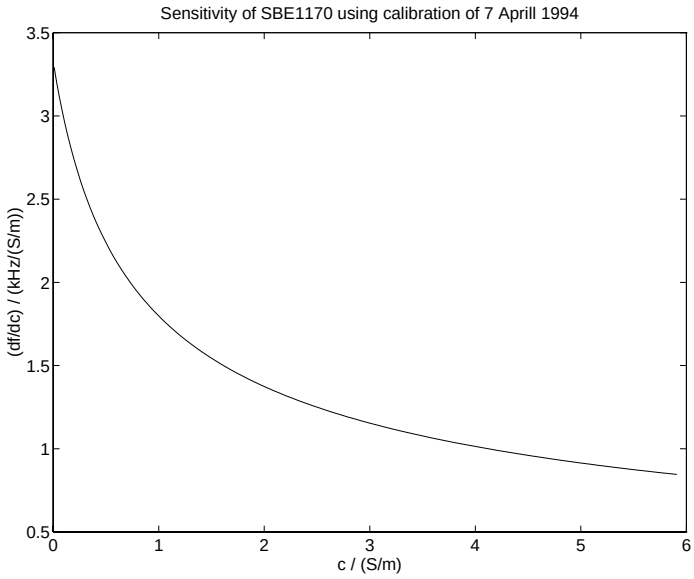

Figure 17: Sensitivity of the Sea-Bird conductivity sensor.

9.1.3 Noise

For period counting *Irish and Levine* (1978) state the theoretical spectral noise level due to least count as (least count)$^2/6$. In a quiet fjord, *Pederson and Gregg* (1979) obtained a spectral noise level of a Sea-Bird conductivity probe of 5×10^{-11} (S/m)^2 Hz^{-1}, which agreed with the theoretical value. It corresponded to an rms value of 1.1×10^{-5} S m^{-1} over a

2.5 Hz bandwidth. Note: *Payne and Smith* (1980) show the digitization noise spectrum is *not*constant with frequency if successive period counting intervals are not separated in time. The digitization error in one interval is correlated with the digitization error in the next.

9.1.4 Dynamic Response

9.2 Data Characteristics

The sample record in Figure 18 has several small spikes of lower conductivity. These appear to result from small particles passing throught the cell and last only one or two scans. They are very hard to detect when they occur in a turbulent section because they may have smaller amplitude than signals. The easiest way to identify them appears to calculate salinity and then first difference. Spikes found so far stand out and can be interpolated across before redoing the salinity calculation.

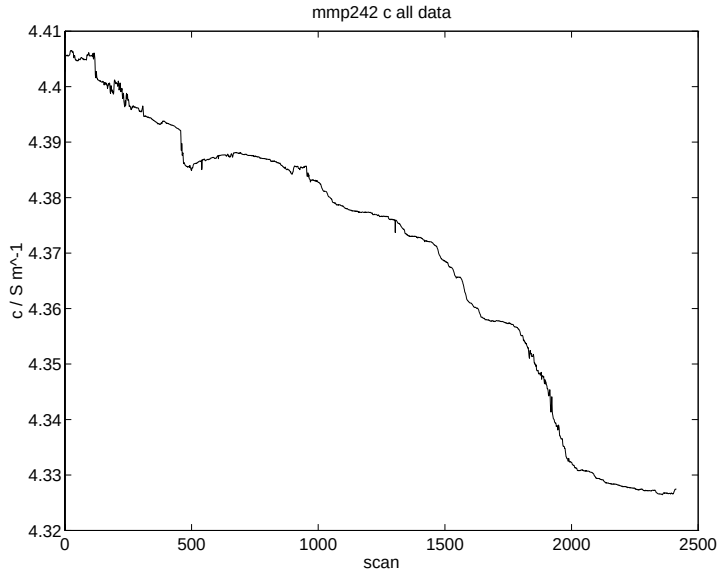

Figure 18: Conductivity from Sea Bird sensor for MMP242.

9.2.1 Noise

MMP3 has not been operated in a place with conductivity levels close to the noise level of the probe. The spectrum in Figure 19 is 10 times the theoretical noise level.

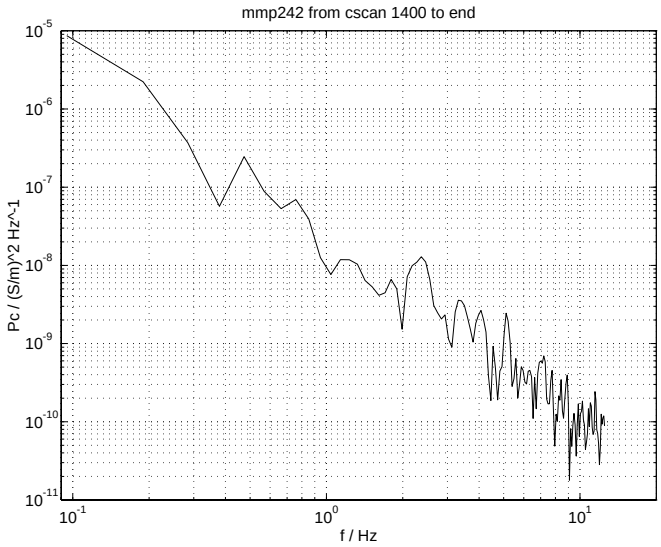

Figure 19: Power spectrum of conductivity for MMP242.

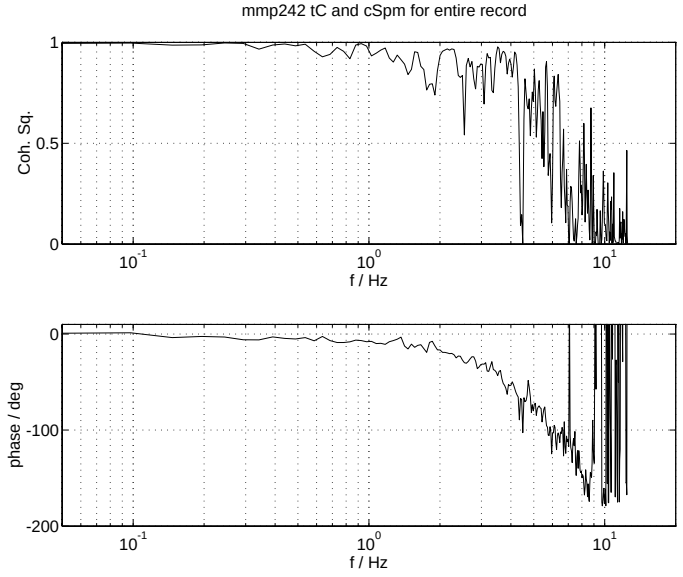

Figure 20: Coherence-squared and phase between Sea Bird temperature and conductivity for MMP242. Temperature was the first record in matlab m file cohere.

10 Optical Backscatter, obs

10.1 Sensor Characteristics

Water turbudity is measured with an obs-3 unit made by D & A Instrument Company, 218 Polk Street, Port Townsend, WA 98368 (phone: 800/437-8352, fax: 206/ 385-0460).

The unit consists of a diode that emits a high intensity infrared beam. Half-power of the beam occurs at 50°in the axial plane of the sensor and 30°in the radial plane. Four photodiodes detect backscattered light between 140°and 160°?? Visible light is attenuated by a filter that transmits less than 1% of incident light with wavelength less than 790 nm.

The frequency response is stated to be 10 Hz, and it has an internal 8-pole Bessel filter that is attenuated by 3 db at 20 Hz.

The dynamic range is 0.02 to 2,000 FTU (Formazin Turbudity Units). From 0 to 2,000 FTU the nonlinearity of the output is less than 2%.

The sensitivity depends on gain, G, which can be 4, 15, or 54.

10.2 Data Conversion

The output, V, is 0 to +5 volts and is related to Formazin Turbudity Units by

$$FTU = 1600V/G \ . \tag{38}$$

Because we are greatly oversampling, we will want to decimate the output.

10.3 Data Characteristics

A typical record is shown in figure 21.

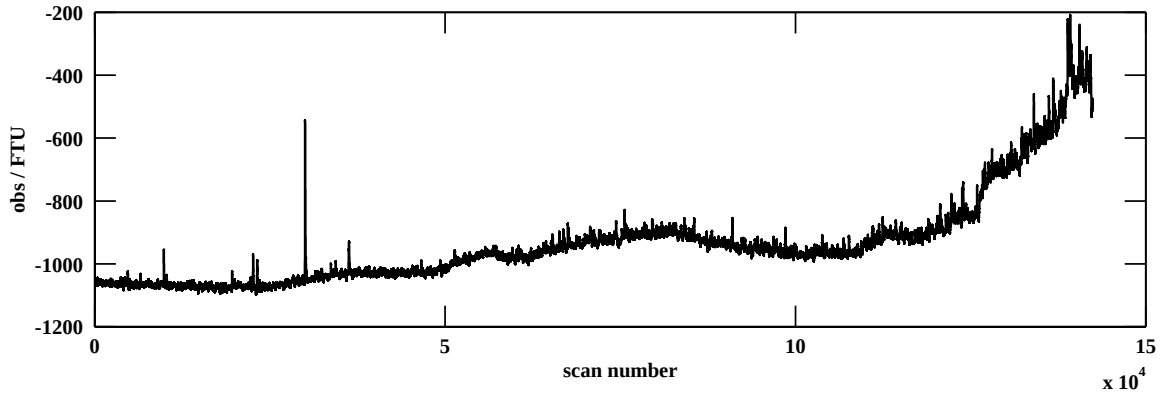

Figure 21: Example of data from the obs channel.

11 Pressure, pr

11.1 Sensor Description

The pressure gauge is a Digiquartz unit model 2500A made by ParosScientific, 4500 148th Ave., N.E., Redmond, WA, 98052. As fractions of full scale, the units is rated as having repeatability and hystersis of $\pm 5 \times 10^{-5}$, and acceleration sensitivity of $\pm 3.8 \times 10^{-5}$ per g. Absolute stability is 1×10^{-4} over three years for temperatures between -54°Cand +55°C. When a temperature compensation equation is provided, the maximum temperature sensitivity is $\pm 8 \times 10^{-6}$ per °C.

Its range is 0 to 500 psia (0 to 3.45—MPa absolute) and the gauge can be overpressured by 20%. The operating range is -40°C to +107°C.

The output is a frequency-modulated square wave of 4 volts peak-to-peak. The pressure signal modulates the signal about 10% within the band of 30–42 kHz.

The pressure gauge contains internal temperature sensors, but initially our units were not calibrated for temperature.

11.1.1 MMP1 History

Initially, MMP1 had Lucas Schavitz strain gauge (serial 164234) that could sense pressures between 0 and 3.50 MPa. The first drops were 9–11 on Nov 9, 1993. This gauge was used during FLIP94 and FLIP95, through drop 2098. After FLIP95, mmp1 was completely reworked, and the strain gauge was replaced by Paros60094. It was first used for drop 2099 in July 1995, and is still in use.

11.1.2 MMP2 History

MMP2 began with Paros 60096 with drop 2099 in July 1995. This gauge is still in use.

11.1.3 MMP3 History

When constructed in July 1996, MMP3 was outfitted with Paros62793 which soon flooded and was ruined. It was replaced with Paros1632 (900 psia range)

On 19 March 1997 Paros 62954 was first used with drop 4187.

11.2 Data Conversion

The frequency is counted in the same manner as the SeaBird temperature and conductivity and is described in Section 5. For the initial configuration (July 1995 to the present, including drops after 2100) the period counter had a reference frequency of $f_r = 8.192$ MHz. Consequently, the period for the ith scan, T^i, is

$$T^i = 10^6(327,680 + N_r^i - N_r^{i-1})/(f_r N_s^i) \quad [\mu\text{s}] \tag{39}$$

where N_r^i and N_s^i are the reference and sensor counts for the ith scan, and N_r^{i-1} is the reference count for the previous scan.

Sea pressure is obtained as

$$pr = C\left(1 - T_0^2/T^2\right)\left(1 - D(1 - T_0^2/T^2)\right) \times 6.894757 \times 10^{-3} - 0.101325 \quad \text{[MPa]} \; . \tag{40}$$

For the initial gauges in MMP1 and MMP2, C, D, and T_0 are the constants given in Table 6.

Gauge	Date	Source	C psia	D	T_0 μs
1632	09jun95*	ParosScientific	5065.546	0.020910	25.51955
1654	09jun95*	ParosScientific	5947.664	0.022484	23.91989

Table 6: Calibration constants for ParosScientific pressure gauges. * Calibrations were obtained at a temperature of 21.0°C.

The next set of Paros gauges have a second analog channel that gives temperature at the gauge, T_p. This temperature is used to compute the coefficients as,

$$C = C_1 + C_2 T_p + C_3 T_p^2 \tag{41}$$

$$D = D_1 + D_2 T_p \tag{42}$$

$$T_0 = T_1 + T_2 T_p + T_3 T_p^2 + T_4 T_p^3 + T_5 T_p^4 \tag{43}$$

Tables 7 and 8 contain these constants.

Gauge	Date	Source	C_1	C_2	C_3	D_1	D_2
60094	08aug95	Paros	2066.999	-9.10985E-3	-2.50503E-4	0.016363	0
60095	08aug95	Paros	2087.691	-1.13400E-2	-2.90016E-4	0.018250	0
62793	02feb96	Paros	2042.320	8.34901E-4	-2.22157E-4	0.015498	0
62954	27feb97	Paros	1984.554	1.29311E-3	-2.57585E-4	0.010292	0

Table 7: Calibration constants for ParosScientific pressure gauges.

Gauge	Date	Source	T_1	T_2	T_3	T_4	T_5
60094	08aug95	Paros	27.92309	-7.12635E-5	1.06989E-6	1.28205E-9	0
60095	08aug95	Paros	27.77493	-6.05344E-5	9.86976E-7	1.75148E-9	0
62793	02feb96	Paros	27.77244	-7.12999E-5	9.57764E-4	1.71152E-9	0
62954	27feb97	Paros	27.77325	-8.47029E-5	1.02120E-6	1.75603E-9	0

Table 8: Calibration constants for ParosScientific pressure gauges.

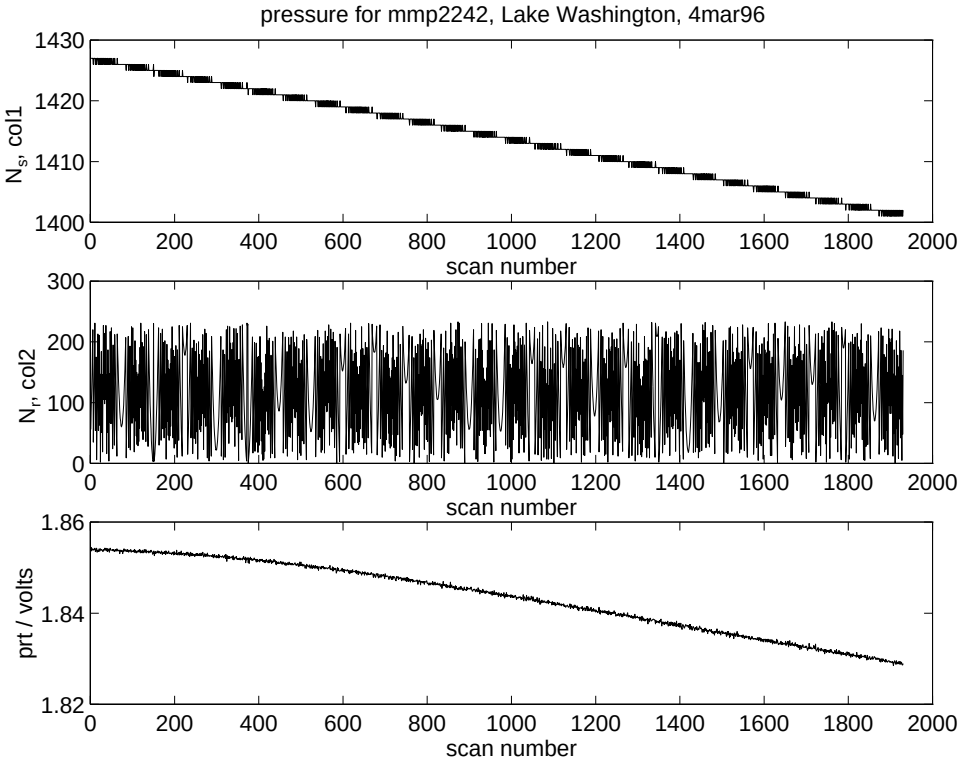

Figure 22: Raw recorded data for pressure (upper two panels) and temperature at the pressure gauge (lower panel). When converted,the temperatures decreased from 21.3°C to 20.2°C.

Figure 22 shows both of the raw channels of pressure counts for a short drop in Lake Washington. The lower panel contains the internal temperature of the gauge from the same profile. During the drop the external temperature decreased from 21.3°C to 20.2°C.

The newest pressure gauges also output their temperature as an analog signal. We digitize it and assign it the mnmenonic 'prt'.

$$T_p = \frac{V - 1.375}{0.0225} \ . \tag{44}$$

11.3 Data Characteristics

Figure 23 has the same data as in Figure 22 after they are converted to MPa in the upper panel. The lower panel has the first-difference of the pressures. Over 10% of the samples are negative owing to the large noise.

Spectra of the converted pressure and internal temperature are shown in Figure 24. The pressure spectrum is dominated by noise for $f > 1$ Hz. The rises at higher frequencies is characteristic of data from period counters. The temperature spectrum appears noisy at all frequencies.

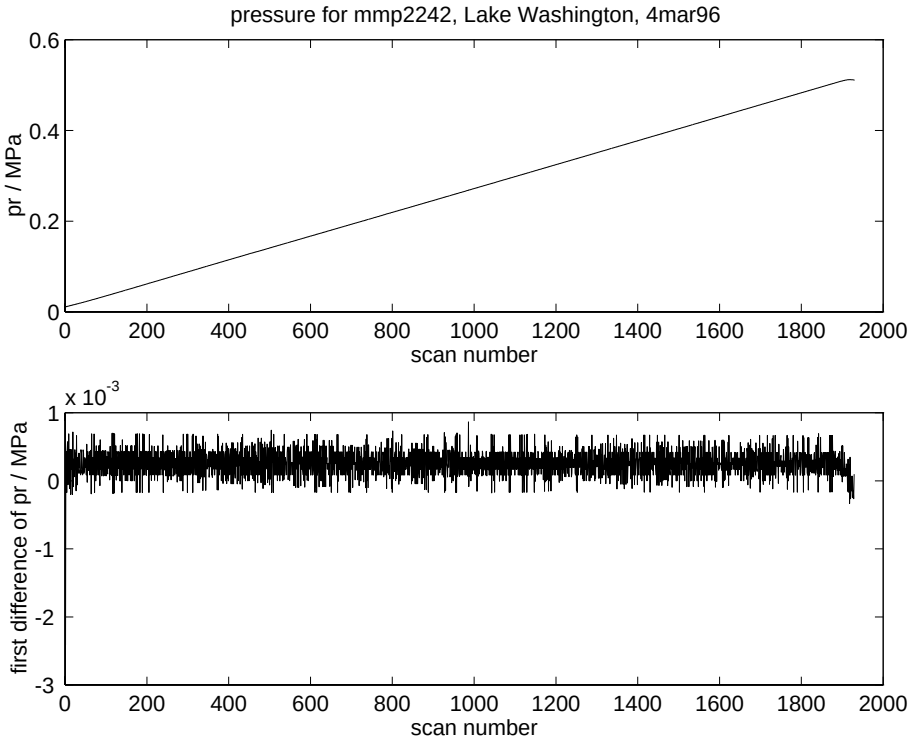

Figure 23: Converted pressure (upper) and its first difference (lower). The recording continued for a few seconds after the instrument started rising.

Because the pressures are so noisy, they will be routinely filtered. Figure 25 compares the initial points in the filtered and original records, when a 4-pole Butterworth filter was used with a cutoff frequency at 1 Hz. Note that the first raw point is bad, as is always the case using this period counting scheme. First differencing produces the smooth plot in the lower panel. It is negative only at the end, when the mmp was ascending. The effect of filtering is shown by the second spectrum in Figure 24.

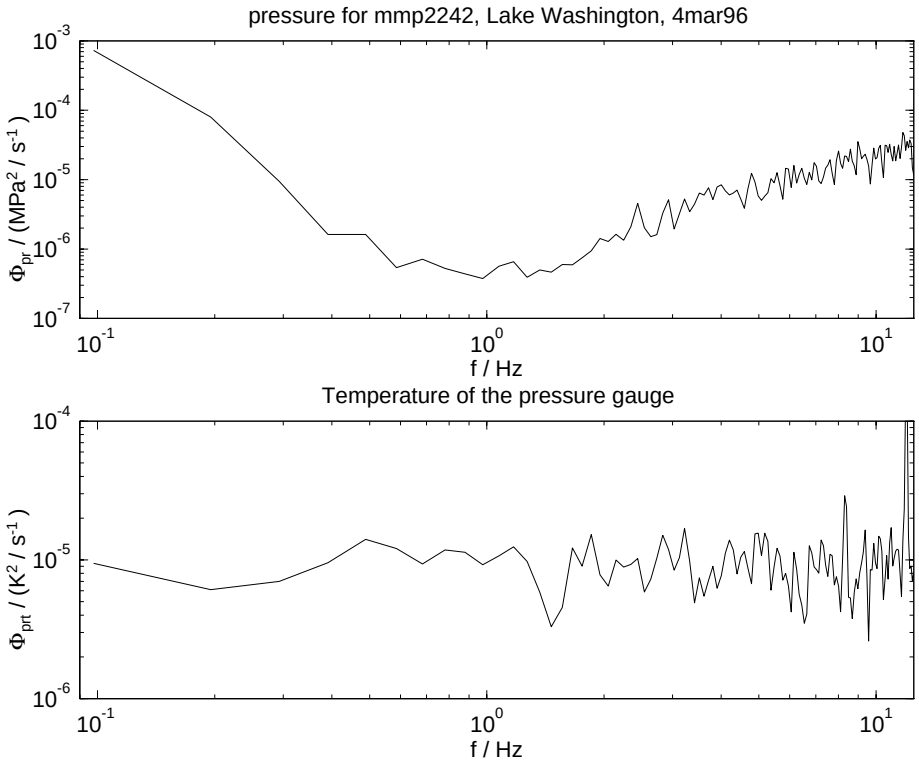

Figure 24: Spectra of converted pressure (upper) and temperature (lower). The upper panel also has the spectrum of pressure after low-pass filtering with a 1 Hz cutoff frequency.

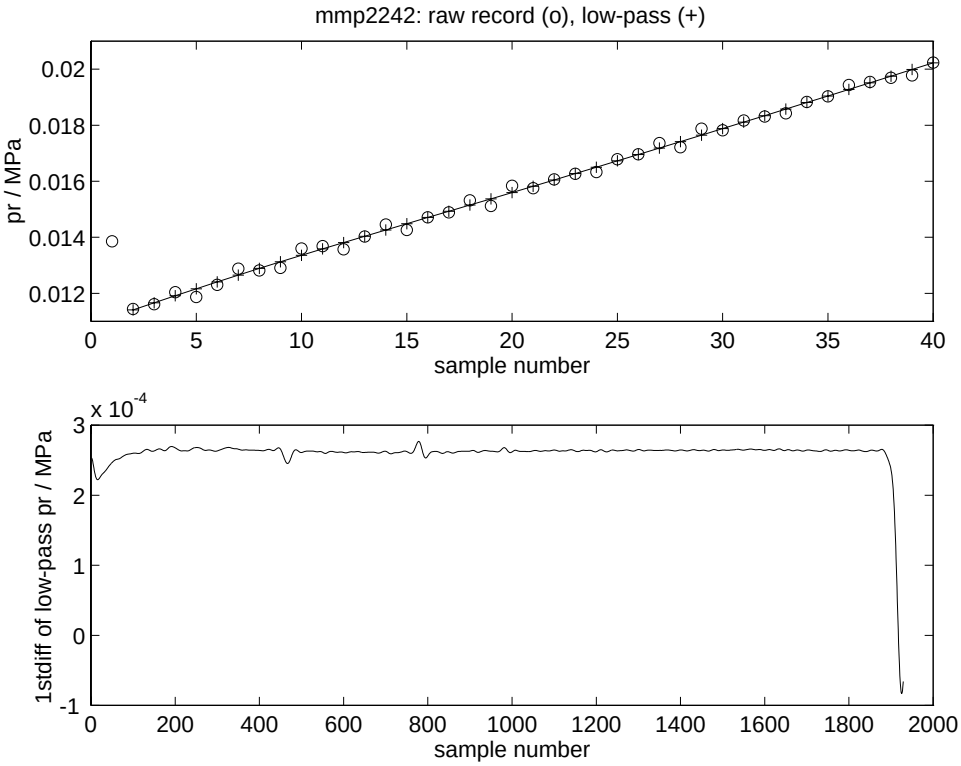

Figure 25: The upper panel compares of the first 40 pressure values before (o) and after low-pass filtering. The first point, however, was not included in the data that were filtered. The lower panel shows the first difference of the low-passed data.

12 Scan Count, sc

The scan count is kept in the middle 12 bits of a 16-bit register, which has the two lowest and the two highest bits set to 0. Consequently, the scan count runs from 0 to $2^{14} - 2^2 = 16,384$. An example is shown in Figure 26. The counter starts from 0 when MMP is turned on.

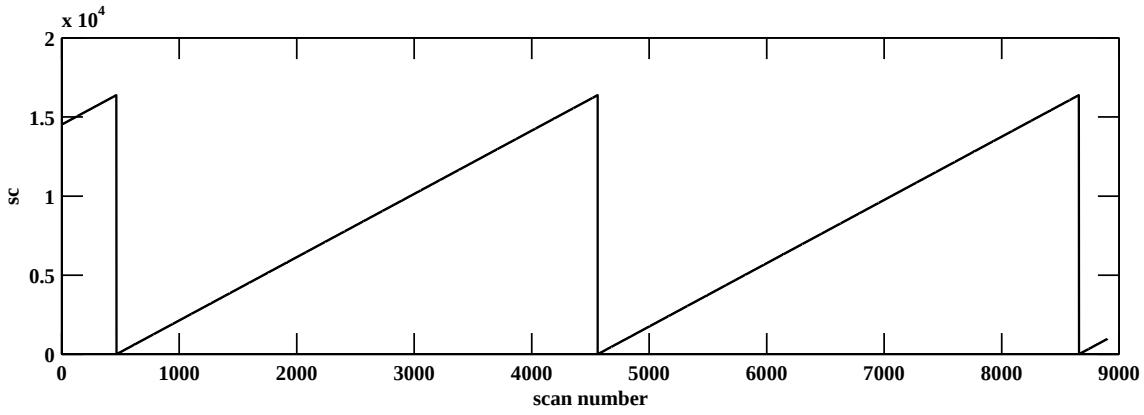

Figure 26: Example of data from the sc channel.

Because drops start later, with no reset applied to the scan counter, data records can begin anywhere in the allowed range. Sequential scan counts increase by 4, retaining the scheme used in AMP.

13 Temperature (low pass), tl1 and tl2

13.1 Sensor Description

These circuits use the same thermistor as the th1 channels; tl1 uses th1, and tl2 uses th2 if the second pair are installed. The thermistors are Thermometrics FP07s with nominal resistances of 820 kΩ at 25°C. *Bennett* (1972) shows that the temperature of glass-encapsulated thermistors is modeled accurately by a third-order polynomial in $\ln(R_T/R_0)$, where R_T is the thermistor resistance and R_0 is a reference resistance. We have found that a second-order polynomial of the same form works just as well and use

$$T = \sum_{i=0}^{i=2} \left(c_i \ln(R_T/R_0)^i \right) - 273.15 \quad [^\circ\mathrm{C}] \; , \tag{45}$$

where $R_0 = 2.5 \times 10^6$ Ω. The dynamic response of the thermistors is dicussed in Section 15.

The sensitivity of a thermistor to temperature is

$$\alpha_T \equiv \frac{1}{R_T} \frac{d\,R_T}{d\,T} \quad [\mathrm{K}^{-1}] \; . \tag{46}$$

Typical values are about -0.05 °C^{-1}.

13.2 Electronics

The combined circuit for high and low-pass temperature is shown in Figure 27, and component values are given in Table 9.

Component	Value	Component	Value
R_1	1.0×10^4 Ω	R_9	1.0×10^4 Ω
R_2	1.0×10^6 Ω	R_{10}	2.5×10^4 Ω
R_3	1.5×10^3 Ω	R_{11}	5.00×10^5 Ω
R_4	1.5×10^3 Ω	R_{12}	5.0×10^4 Ω
R_5	4.99×10^5 Ω	C_3	2×10^{-6} F
R_6	1.0×10^6 Ω	C_8	2×10^{-6} F
R_7	1.3×10^3 Ω	C_9	2×10^{-6} F
R_8	4.99×10^5 Ω	C_{10}	2×10^{-6} F
E_0	nominally 10 V		

Table 9: Values of circuit components used with the high and low-pass temperature circuits.

Specifications for the voltage reference, E_0, are 9.9995 to 10.005 volts. In 1994 they were measured as 9.9992 (case t1) land 10.0003 (case t2). Temperature sensitivity is specified as 5 ppm/°Cmaximum and 2 ppm/°C typical.

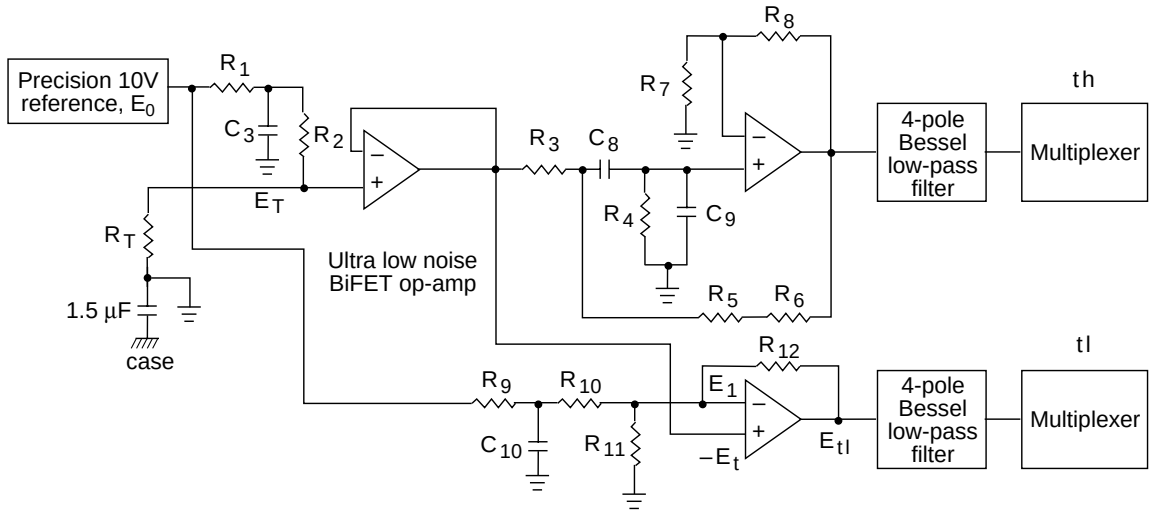

Figure 27: Circuit diagram for high and low-pass temperature. Both circuits use the same thermistor, indicated by resistance R_T.

The precision 10 volt reference source, E_0, is nominally 10 volts and produces a voltage across the thermistor, R_T, of

$$E_T = \frac{R_T}{R_1 + R_2 + R_T} E_0 \quad [\text{volts}] \ . \tag{47}$$

The change of this voltage with temperature is

$$\beta \equiv \frac{dE_T}{dT} = \frac{\alpha_T (R_1 + R_2) R_T E_0}{(R_1 + R_2 + R_T)^2} \quad [\text{V K}^{-1}] \ . \tag{48}$$

E_T is fed to a buffer amplifier that produces a low-impedance output, which is fed to the positive input of the low-pass OpAmp. The resistors are adjusted to match E_T at the middle of the expected range for oceanic temperatures.

The output voltage is

$$E_{tl} = G_{tl} E_T - E_1 \ , \tag{49}$$

where

$$E_1 = \frac{R_{12}}{R_9 + R_{10}} E_0 \ , \tag{50}$$

and G_{tl} is the gain,

$$G_{tl} = 1 + \frac{R_{12}}{R_{11}} + \frac{R_{12}}{R_9 + R_{10}} = 2.529 \ . \tag{51}$$

13.3 Data Conversion

13.3.1 Volts to °C

In-situ calibrations are done by aligning and then fitting the Sea-Bird temperature, tC, to low-pass temperature in volts, tl1V. The polynomial coefficients are then used to convert tl1 from volts to °C, e.g.

$$T = a_1 E_{tl}^2 + a_2 E_{tl} + a_3 \quad [^\circ\mathrm{C}\ ] \ . \tag{52}$$

For mmp242 a second-order fit appeared optimum. The coefficients were
$a_1 = -4.8874815733149707e-01$, $a_2 = -4.6070128816818681e+00$,
and $a_3 = 8.8987025287198858e+00$. The fit is quite good over most of the record, but some residuals are 0.03°C (Fig. 28). These appear to result from three anomalies between the two

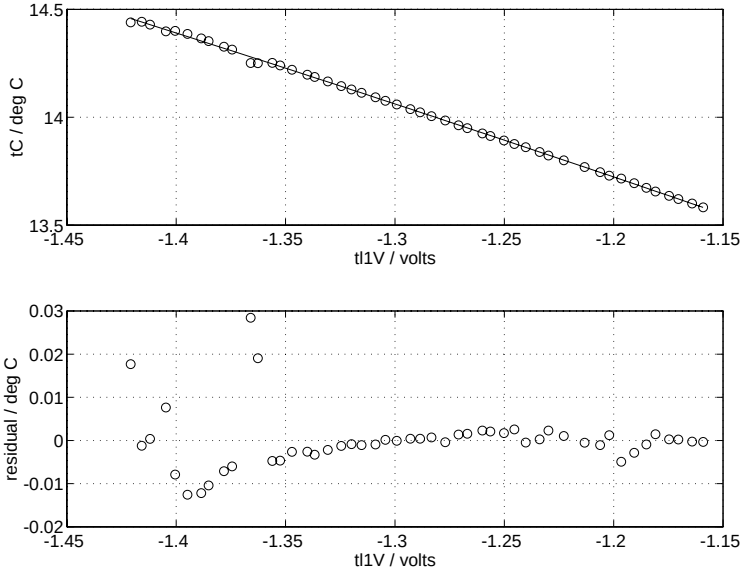

Figure 28: Fit and residuals for tC as a function of tl1V for mmp242. The data were sorted into 50 bins by voltage. Bins with fewer than 5 samples were not used for the fit.

records in the first 10,000 scans (Fig. 29). We suspect that these are electronic, as the one at scan 1,000 contains 25 Hz oscillations.

13.3.2 Calculation of β

By using SeaBird temperature as a reference, T, voltage output from the tl circuit can be used to compute β. Taking $tl1V$ as recorded volts from tl1, the first step is to compute E_T, the voltage across the thermistor,

$$E_T = \frac{tl1V + E1}{G_{tl}} \ . \tag{53}$$

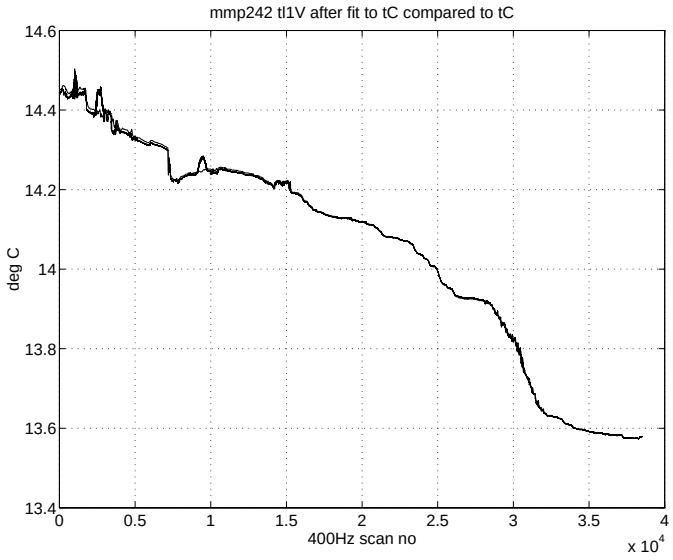

Figure 29: Converted tl1 overlaid with Sea-Bird temperature. Major disagreements occur at scans 1,000, 3,000 and 9,500. The first is a burst of 25 Hz pickup.

A second order fit of E_T to T is then done using Matlab,

$$E_{T\text{fit}} = \text{polyfit}(T, E_T, 2) \ . \tag{54}$$

Evaluating the fit,

$$E_{T\text{calc}} = \text{polyval}(E_{T\text{fit}}, T) \ , \tag{55}$$

followed by first-differencing and dividing

$$\beta = \frac{\text{diff}(E_{T\text{calc}})}{diff(T)} \ . \tag{56}$$

13.3.3 Temperature Spectra From Raw Data

Spectra should usually be taken after the raw data have been converted to temperature using the fits to the Sea-Bird temperatures. If, however, spectra are desired from the raw data, the spectrum of the recorded data is

$$\Phi_{\text{R}}(f) = \beta^2 G_{tl}^2 H_{\text{Bessel4}}^2(f) H_{FP07}^2(f,w) \frac{\Phi_T(k_3)}{w} \quad [\text{V}^2 \ \text{Hz}^{-1}] \ . \tag{57}$$

Inverting gives the temperature spectrum,

$$\Phi_T(k_3) = \frac{w}{\beta^2} \frac{\Phi_{\text{R}}(f)}{H_{\text{Bessel4}}^2(f) H_{\text{FPO7}}^2(f,w) G_{tl}^2(f)} \quad [\text{K}^2 \ \text{cpm}^{-1}] \ . \tag{58}$$

Because resistance changes of the thermistor are relatively large, β should be evaluated for each spectral block.

The spectrum of temperature gradient is

$$\Phi_{\partial T/\partial z}(k_3) = (2\pi k_3)^2 \Phi_T(k_3) \quad [(\mathrm{K/m})^2 \ \mathrm{cpm}^{-1}] \ . \tag{59}$$

These channels are limited by quantization noise at wavenumbers lower than the diffusive cutoff of the temperature spectrum. Therefore, they are not useful for determining χ.

13.4 Observed Characteristics

Figure 3 in Section 3 shows raw data where the amplitudes are close to least count.

Figure 4 shows a spectrum of raw data from a region where signals are relatively weak. The flat noise spectrum at high frequencies is close to the theoretical quantization noise level of 2.45×10^{-11} volts^2 Hz^{-1}.

This is typical of temperature circuits fed into 16-bit A/Ds, as 30 °C/2^{16} = 4.6 m°C. This is often less than the net temperature change over several centimeters.

Figure 30 shows the spectrum of the lower part of the a converted tl1V record. It overlays

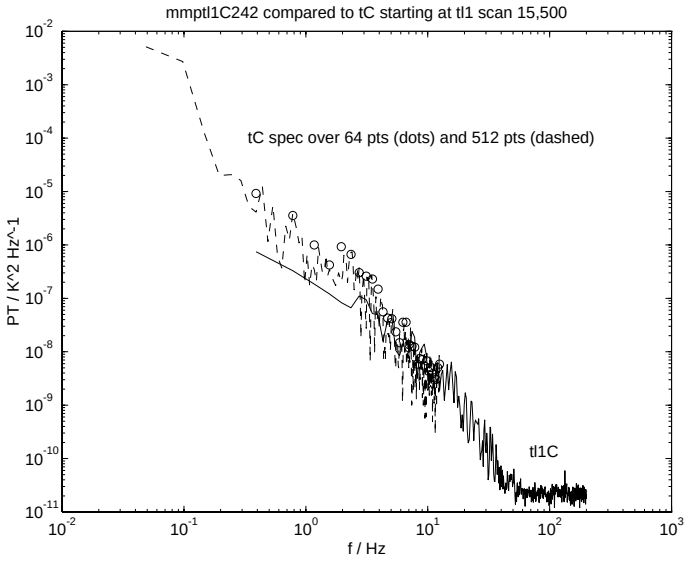

Figure 30: Temperature spectrum of the lower part of tl1C for mmp242 overlaid with spectra of tC. The flat level at high frequencies is the noise level.

the Sea-Bird temperature spectrum, to which it was fitted. As expected, tl has a lower noise floor which is $\approx 2 \times 10^{-11}$ K^2 Hz^{-1}. Integrating i.e. 200 Hz $\times 2 \times 10^{-11}$ K^2 Hz^{-1}, gives an rms noise of 6.3×10^{-5} K^2 Hz^{-1}. The circuit is set up to span 30°C with the 16-bit full output range. Consequently, in terms of temperature the least count is $30°\mathrm{C}/2^{16} = 4.57 \times 10^{-4}$ °C. The ratio, $4.57 \times 10^{-4}/6.3 \times 10^{-5} = 7.2$ demonstrates that the noise is not quite uniformly distributed. If it were, this ratio should be 12 according to (3).

14 Temperature (Sea Bird), t

14.1 Sensor Description

The sensor is a Sea Bird Model SBE-3 oceanographic thermometer, which has a thermistor in one branch of a Wien bridge oscillator circuit to produce a frequency that decreases with increasing thermistor resistance. The thermistor is protected from ambient pressure by a thin-walled stainless steel tube. For our application the thermistor is mounted in the tc duct so it will sample the same water flowing through the conductivity cell (Fig. 15 in Section 9). Full scale is -1°C to 31°C and corresponds to outputs of 6kHz to 12kHz. The output is fed to a period counter and that section should be read to understand the characteristics of period-counted data.

14.1.1 Static Response

The sensors are very stable and have predictable drift rates. Consequently, semi-annual calibrations are adequate. Sea Bird guarantees a stability of ±10 m°C over six months and a resolution of 0.5 m°C when sampled at 12 Hz. The probes are calibrated at 6 or more temperatures between -1°C and 31°C. The following equation, derived from *Bennett* (1972), is used

$$T = \frac{1}{a + b\ln(f_0/f) + c\ln^2(f_0/f) + d\ln^3(f_0/f)} - 273.15 \quad [^\circ\mathrm{C}\ ]\ , \tag{60}$$

where f is frequency in kHz, f_0 is the temperature of the lowest calibration temperature, and the constants are determined from fits. The calibration of probe 1412 on 2 April 1994 gave: $a = 3.68104711 \times 10^{-3}$, $b = 6.01090425 \times 10^{-4}$, $c = 1.53053484 \times 10^{-5}$, $d = 2.29900585 \times 10^{-6}$, and $f_0 = 6170.48$. The frequency, f, is expressed in Hz, and the above calibration is plotted versus temperature in Figure 31

The sensitivity is oftained by differentiating (60),

$$S_{\mathrm{sbeT}} \equiv \frac{df}{dT} = \frac{f\left(a + b\ln(f_0/f) + c\ln^2(f_0/f) + d\ln^3(f_0/f)\right)^2}{b + 2c\ln(f_0/f) + 3D\ln^2(f_0/f)} \quad [\mathrm{Hz\ K^{-1}}]\ . \tag{61}$$

In Figure 32 the sensitivity has been computed by numerically differentiating (60) as plotted in the previous figure.

14.1.2 Dynamic Response

14.2 Data Conversion

The sinusoidal output is converted to a square wave by a zero-crossing detector before digitization with a hybrid period counter.

For raw data expressed as frequencies, the recorded spectrum is

$$\Phi_{\mathrm{R}}(f) = S^2_{\mathrm{sbeT}} \frac{\Phi_T(k_3)}{w} H^2_{\mathrm{sbeT}}(f) \quad [\mathrm{Hz^2\ Hz^{-1}}]\ . \tag{62}$$

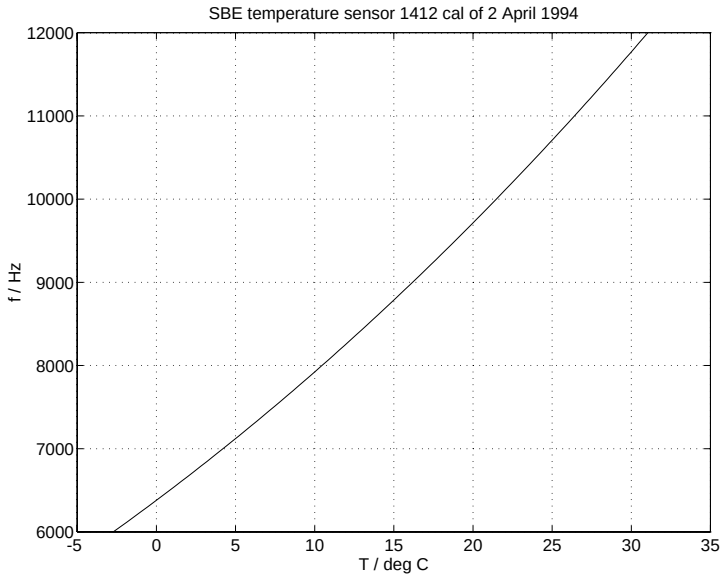

Figure 31: Frequency versus temperature for SBE temperature probe 1412 using the calibration of 2 April 1994.

Figure 32: Typical sensitivity of a Sea-Bird temperature probe. (FIGURE DOES NOT PRINT OR OPEN WITH ILLUSTRATOR OR GSVIEW)

Inverting,

$$\Phi_T(k_3) = \frac{1}{wS^2_{\rm sbeT}} \frac{\Phi_{\rm R}(f)}{H^2_{\rm sbeT}(f)} \quad [{\rm K}^2\ {\rm cpm}^{-1}] \ . \tag{63}$$

14.3 Data Characteristics

Figure 33 shows a complete record taken from FLIP off San Diego. Its spectrum is plotted in Figure 34.

COMPARE NOISE WITH LEAST COUNT FOR PERIOD COUNTING

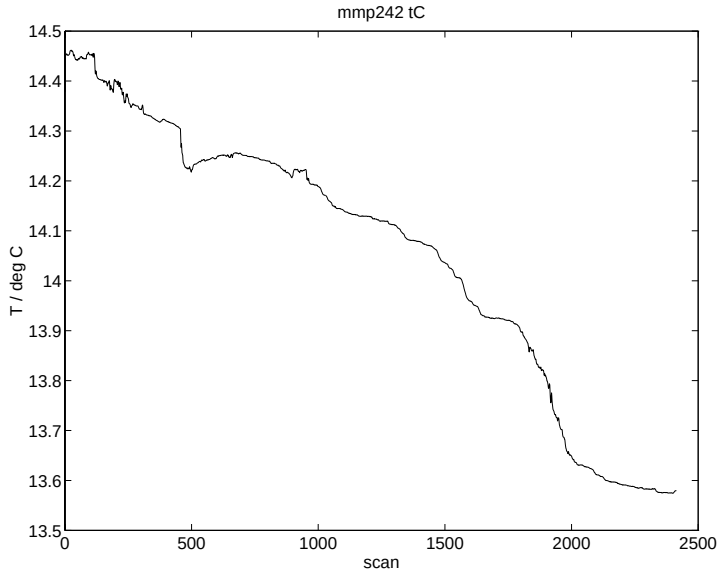

Figure 33: Temperature record from the Sea Bird probe.

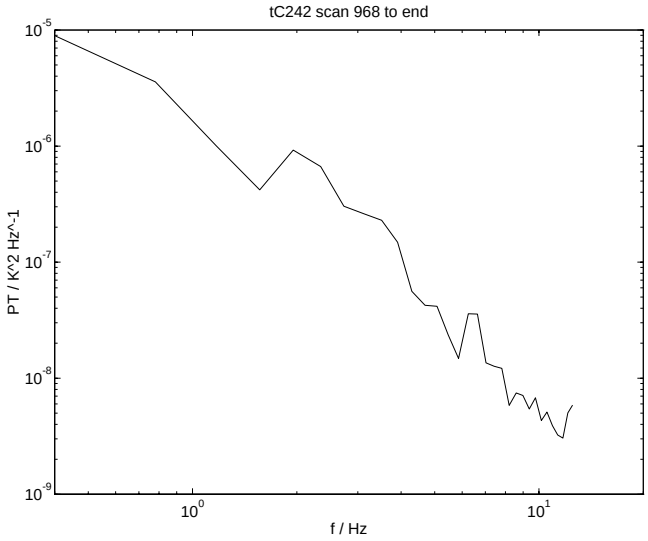

Figure 34: Power spectrum of the Sea Bird temperature channel for MMP242 from scan 968 to the end.

15 Temperature Gradient, th1 and th2

15.1 Sensor Description

The sensor is the same FP07 glasstip thermistor as used for low-pass temperature and described in Section 13.

Nominal dynamic responses are used to correct the frequency response. Based on *Gregg and Meagher* (1980), we assume a double-pole low pass filter with

$$H^2_{\rm FP07}(f,w) = \left(1 + (2\pi f\tau)^2\right)^{-2} \quad , \quad \phi_{\rm FP07}(f,w) = -2\tan^{-1}(2\pi f\tau) \ . \tag{64}$$

The time constant, τ, depends on probe speed, w. We use

$$\tau(w) = 0.005 w^{-0.32} \ [\rm s] \ , \tag{65}$$

with w the fall rate in m s^{-1}. *Gregg and Meagher* (1980) did not report responses for Fasttip thermistors, but several were measured. These showed that the Fasttips also appear to have a double-pole response. The time constant, however, has been adjusted based on both these calibrations and shapes of corrected spectra where the Batchelor spectrum is expected. Hence, the corrections are only approximate, as probe responses differ significantly owing to variations in placement of the thermistor bead in the glass coating and to small air bubbles in the glass.

Figures 35 and 36 show the responses as functions of frequency and wavenumber. Be-

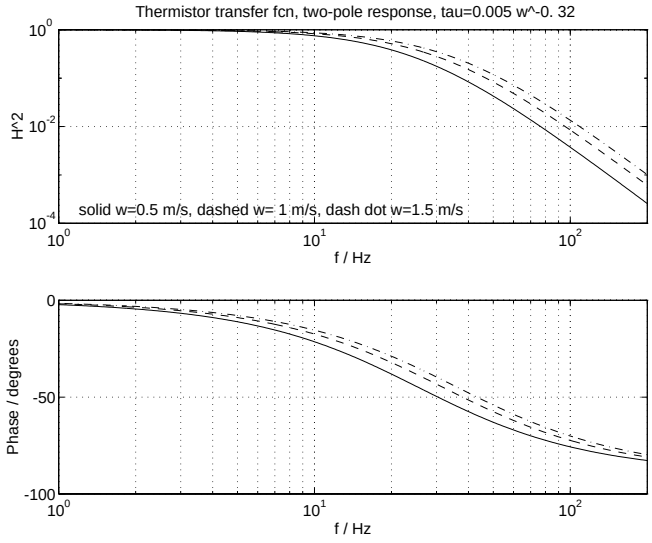

Figure 35: Thermistor responses used with MMP.

cause τ decreases with increasing speed, owing to the boundary layer thinning, the frequency

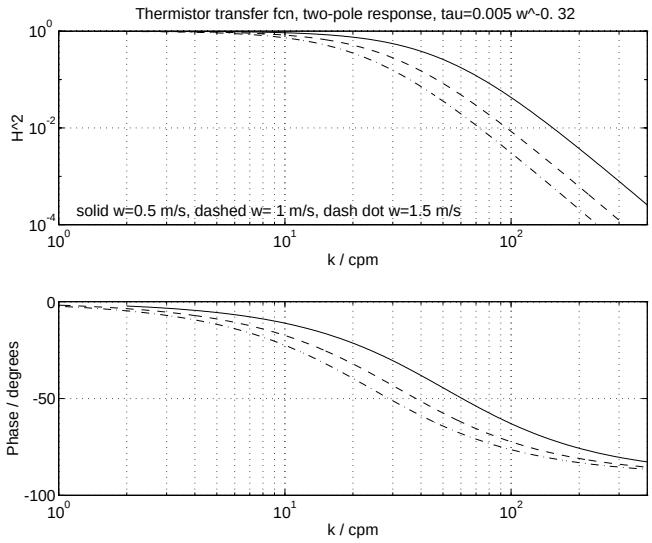

Figure 36: Thermistor responses used with MMP, as functions of wavenumber.

response improves with speed. Spatial resolution, however, decreases. The corrections should not be trusted at wavenumbers greater than 100 cpm and should be considered suspect at even lower wavenumbers.

15.2 Electronics

The circuit diagram and component values are given in Section 13.

The transfer function of the high-pass circuit is given by *Gregg et al.* (1978). Note that component nomenclature and values have changed; the form, however, is the same. For MMP3, the gain is

$$G_{\rm th} = \frac{R_7 + R_8}{R_7} = 500 \ , \tag{66}$$

and the amplitude-squared transfer function is

$$H^2_{\rm hp}(f) = \frac{(2\pi f C_8 R_4 G_{th})^2}{D_1^2 + D_2^2} \tag{67}$$

where

$$D_1 = 1 + \frac{R_3}{R_5 + R_6} - (2\pi f)^2 C_8 C_9 R_3 R_4 \ , \tag{68}$$

and

$$D_2 = (2\pi f)\left(C_8 R_3 + (C_8 + C_9)R_4 + \frac{R_3 R_4}{R_5 + R_6}(C_9 + C_8(1 - G_{th}))\right) \ . \tag{69}$$

Figures 37 and 38 show the total transfer function, including the thermistor response.

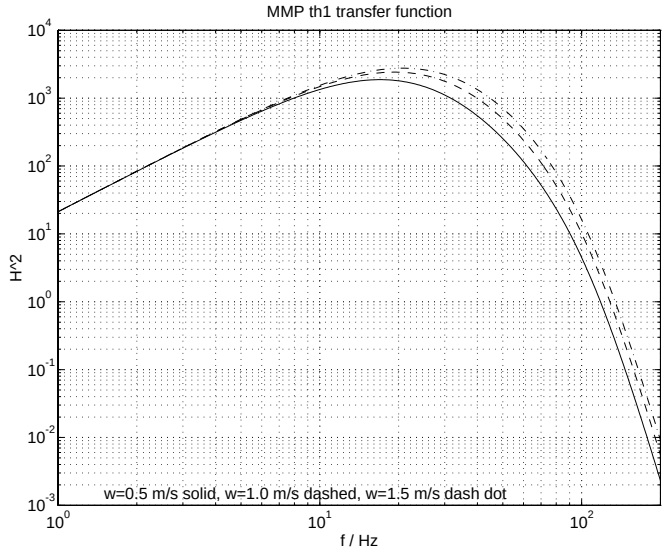

Figure 37: Total transfer function as a function of frequency for three probe speeds. Changes with speed are due solely to the thermistor.

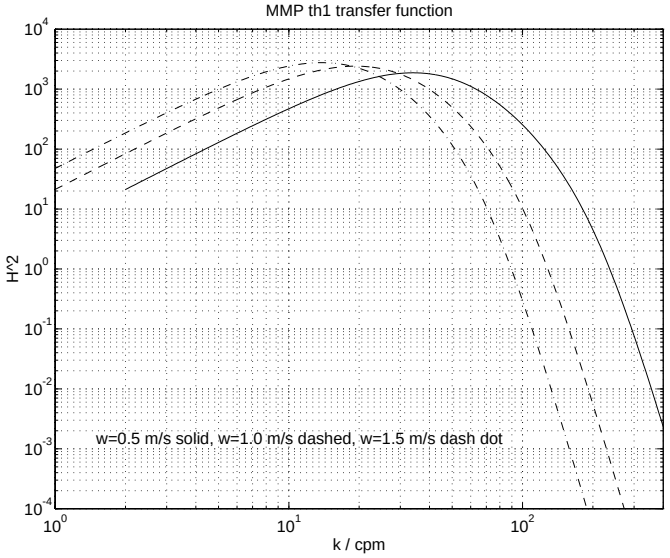

Figure 38: Total transfer function as a function of wavenumber for three probe speeds.

15.3 Data Conversion

The recorded spectrum is

$$\Phi_{\mathrm{R}}(f) = \Phi_T(f) \left(H^2_{\mathrm{hp}}(f) H^2_{\mathrm{Bessel4}}(f) \right) H^2_{FP07}(f, w) \beta^2 \quad \left[\mathrm{V}^2 \ \mathrm{Hz}^{-1} \right] \ , \tag{70}$$

where $\Phi_T(f)$ is the oceanic temperature spectrum as a function of frequency. It is obtained from the oceanic wavenumber spectum by

$$\Phi_T(k_3 = f/w) = w\Phi_T(f) \quad \left[\mathrm{K}^2\ \mathrm{cpm}^{-1}\right] \ . \tag{71}$$

The portion in () is the total electronic transfer function, $H_e^2(f)$.

The temperature spectrum as a function of vertical wavenumber is

$$\Phi_T(k_3) = \frac{w\Phi_\mathrm{R}(f)}{H_e^2(f)H_{FP07}^2(f)\beta^2} \quad [\mathrm{K}^2\ \mathrm{cpm}^{-1}] \ . \tag{72}$$

The temperature gradient spectrum as a function of vertical wavenumber is

$$\Phi_{TG}(k_3) = (2\pi k_3)^2\Phi_T(k_3) \quad \left[(\mathrm{K/m})^2\ \mathrm{cpm}^{-1}\right] \ . \tag{73}$$

The rate of diffusive smoothing of temperature fluctuations is

$$\chi_T = (1-3)2\kappa_\mathrm{T}\int_0^{k_u}\Phi_{TG}(k_3)d\,k_3 \quad \left[\mathrm{K}^2\ \mathrm{s}^{-1}\right] \tag{74}$$

where the factor (1–3) is the degree of isotropy of the temperature gradients in the dissipation range. We use 3 for full isotropy. DISCUSS CUTOFF.

The temperature dissipation spectrum is

$$\Phi_\mathrm{Tdiss}(k_3) = (2\pi k_3)\Phi_{TG}(k_3) \quad \left[\mathrm{K}^2\right] \ . \tag{75}$$

To display contributions to χ_T in 'variance-preserving' form, $\Phi_\mathrm{Tdiss}(k_3)$ is plotted on a linear y-axis versus a logarithmic x-axis.

15.4 Observed Characteristics

Figure 39 shows a typical th1 record. A spectrum from near the end, where activity is minimal, shows that the channel is sometimes not limited by quantization noise (Fig. 40).

Figure 41 compares temperature spectra from th1 and tl1 for the same record. In this case, th1 gives only marginally lower noise. This needs to be checked where the mean gradient is much smaller, as it is possible that th1 does not have the expected low noise found with the same circuit in previous instruments.

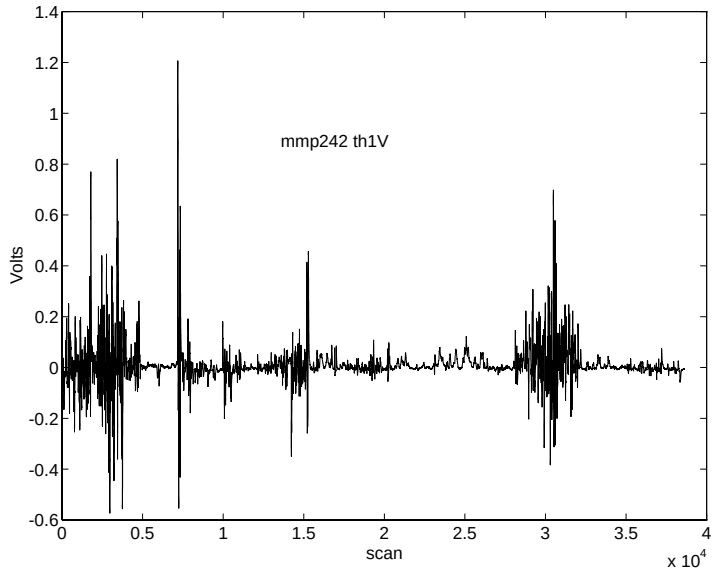

Figure 39: All th1 points for mmp242.

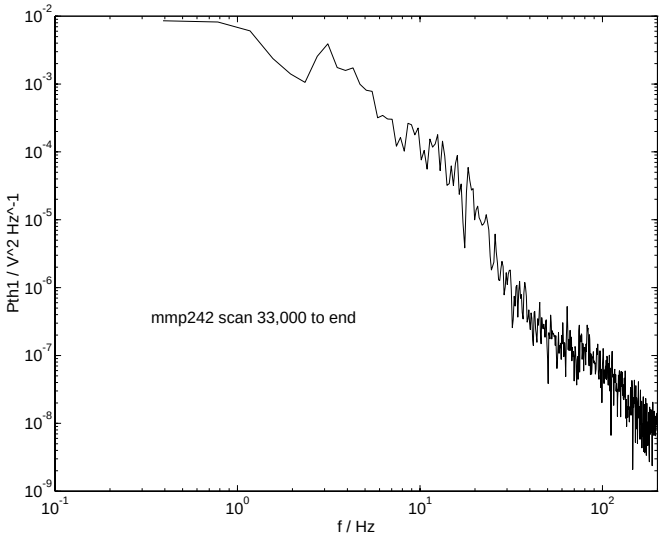

Figure 40: Power spectrum of th1 for mmp242. The spectrum is not limited by quantization noise.

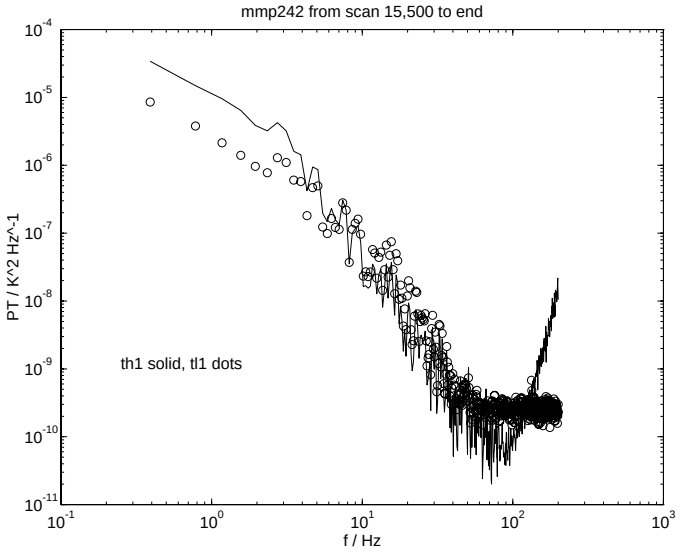

Figure 41: Temperature spectrum from th1V overlaid with tl1 from the same section. Th1 was corrrected using nominal thermistor parameters.

16 Velocity, v1 and v2

16.1 Sensor Description

The airfoil probes are constructed in the manner developed by *Oakey* (1977) and shown in Fig. 42. One end of a bimorph beam is potted directly in hard epoxy, and the remainder

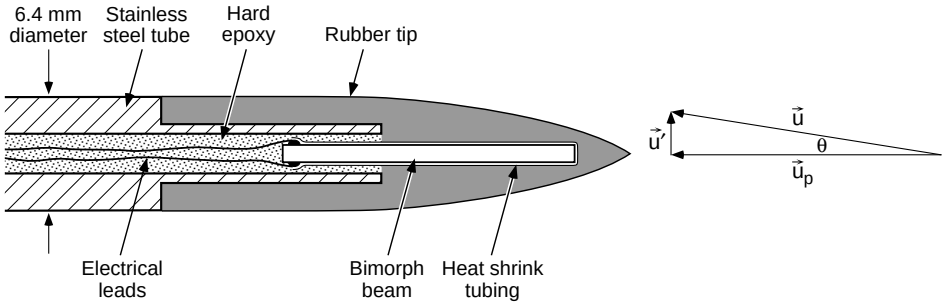

Figure 42: Schematic of airfoil probe used on MMP. For MMP, the probe velocity is the fall rate, w, and u' is any horizontal velocity relative to the MMP.

is encased in the soft rubber tip. The beams have high impedance, with resistances of about 10^{13} Ω, and capacitances of $C_S \approx 1000$ pF. Bending a beam in the direction of its sensitive axis produces a voltage. *Osborn and Crawford* (1980) describe the probes and their sensitivities. MMP3 carries two airfoils, both oriented with their sensitive axis in the same direction so their outputs can be compared during data editing; impacts of plankton on the probes are major causes of noise, and few impacts are simultaneous on both probes.

The rubber tips are made with parabolic cross-sections to provide constant lift for velocities u' parallel to the sensitive axis. The output voltage is

$$E_0(t) = S_v \left(\frac{V^2}{2g}\right) \frac{u'(t)}{V} \quad [V] \,, \tag{76}$$

where S_v is the probe sensitivity, and g is the gravitational constant. Typical sensitivities are $S_v = 18$ to 30 volts per meter.

The probes must be calibrated before and after cruises. This consists of measuring C_S with a precision capacitance meter and determining S_v using Oakey's procedure of placing them in a steady water jet having speed V. Slowly oscillating the probes creates a cross-velocity by changing the angle of attack, θ. Owing to the small angles, $u'(t)/V \approx \sin\theta(t)$. In practice, $\theta(t)$ and $E_0(t)$ are sinusoidal, and S_v is determined from their peak amplitudes. As shown below, the probe capacitance, C_S, also affects gain and must be measured. The nominal capacitance is 1000 pF. Probe sensitivities and capacitances measured before and after the cruise typically differ less than 15%.

Oakey (1977) estimates the dynamic response of the airfoil probes as

$$H^2_{\rm Oakey}(f,w) = \frac{1}{1+(\lambda_{\rm c} f/w)^2} \quad , \quad \phi_{\rm Oakey}(f,w) = \tag{77}$$

with $\lambda_c = 0.02$ m and $k_3 = f/w$, which is the vertical wavenumber in cycles per meter (cpm). Based on laboratory comparisons with a laser Doppler velocimeter, *Ninnis* (1984) gives the transfer function as

$$H^2_{\text{Ninnis}}(f, w) = A_0 + x\left(A_1 + x\left(A_2 + x(A_3 + xA_4)\right)\right) \ , \tag{78}$$

where $x \equiv f/(wK_0)$. It is meant to be used only to 100 cpm, corresponding to 60 Hz at a typical fall rate of 0.6 m s^{-1}. The parameters are given in Table 10, and both probe responses are shown in Figure 43. We use the Oakey version.

Parameter	Value
K_0	140.0
A_0	1.000
A_1	-0.165
A_2	-4.763
A_3	5.900

Table 10: Parameter values for Ninnis's representation of the airfoil transfer function.

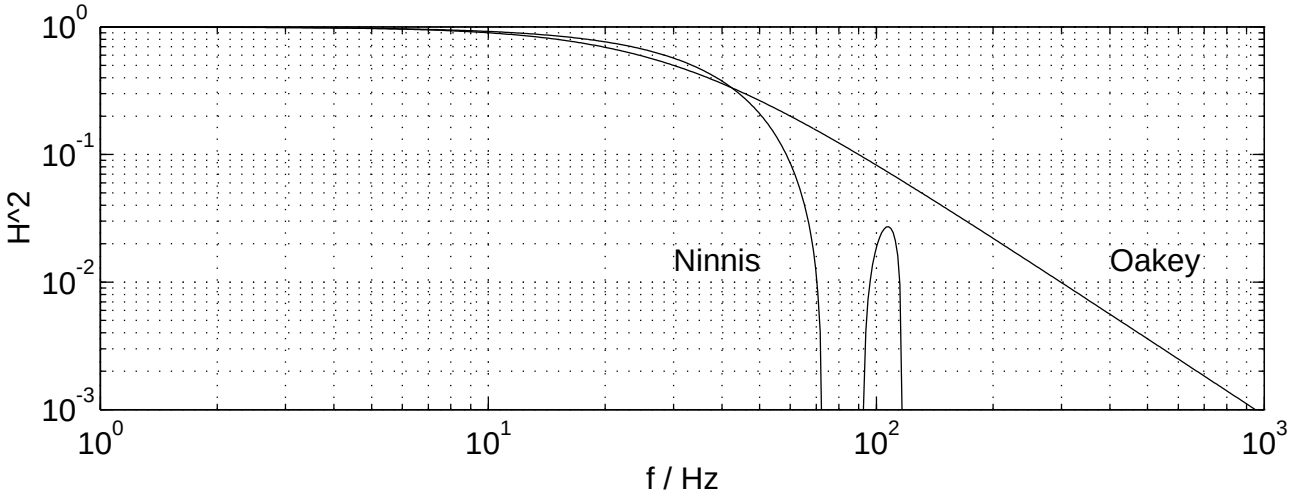

Figure 43: Transfer functions of the airfoil probe, with $w = 0.6$ m s^{-1}.

16.2 Electronics

The airfoil output voltage, E_0 is fed into three sequential circuits that buffer, differentiate, and amplify the signal (Figure 44). Circuit parameters are listed in Table 11.

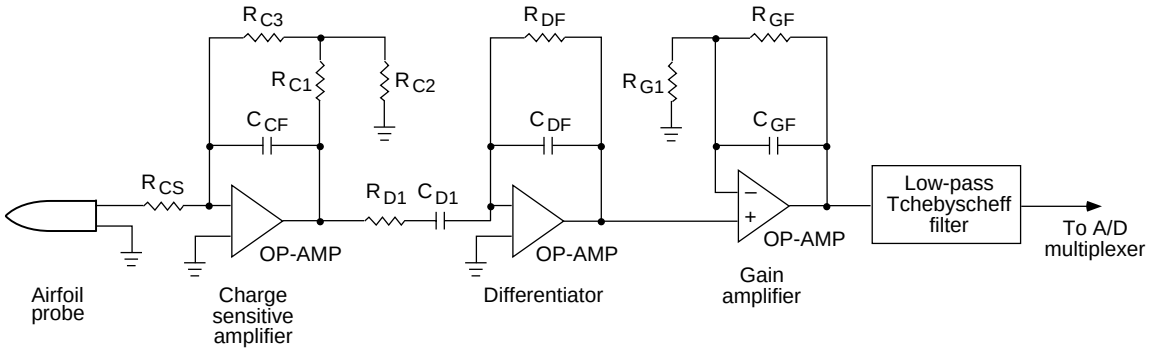

Figure 44: Schematic of airfoil circuits. The probe capacitance, C_S is between R_{CS} and common.

Component	Value	Component	Value
R_{C1}	$1 \times 10^6\ \Omega$	R_{DF}	$4.75 \times 10^5\ \Omega$
R_{C2}	$3.01 \times 10^3\ \Omega$	C_{DF}	8.2×10^{-10} F
R_{C3}	$1 \times 10^7\ \Omega$	R_{G1}	$1.21 \times 10^4\ \Omega$
C_{CF}	1×10^{-9} F	R_{GF}	$3.74 \times 10^4\ \Omega$
R_{D1}	$2.37 \times 10^3\ \Omega$	R_{CS}	$1 \times 10^5\ \Omega$
C_{D1}	3.3×10^{-7} F		

Table 11: Values of circuit components used with the airfoil probes.

The first stage is a charge-sensitive amplifier whose output matches its input voltage while supplying the current needed by the second stage. The power transfer function of the charge amplifier is

$$H^2_{\rm ca}(f, C_S) = \frac{(C_S/C_{CF})^2 (f/f_L)^2}{(1 + (f/f_L)^2)\,(1 + (f/f_H)^2)} \quad , \quad \phi_{\rm ca} = , \tag{79}$$

where

$$R_{\rm f} \equiv \frac{R_{C1} R_{C3}}{R_{C2}} = 3.32 \times 10^9\ \Omega \quad , \quad f_L \equiv (2\pi R_f C_{CF})^{-1} = 0.0479\ \text{Hz} \ , \tag{80}$$

and

$$f_H = (2\pi R_{CS} C_S)^{-1} \approx 1592\ [\text{Hz}] \ . \tag{81}$$

The response is unity at frequencies resolved by the airfoil probes and rolls off at lower and higher frequencies. The high-frequency rolloff is so much larger than frequencies of interest, that the term can be treated as a constant rather than being evaluated with C_S for each probe.

The second stage differentiates frequencies less than 100 Hz,

$$H^2_{\rm diff}(f) = \frac{K^2 f^2}{(f_1^2 + f^2)(f_2^2 + f^2)} \quad , \quad \phi_{\rm diff}(f) = \tan^{-1}\left(\frac{f_1 f_2 - f^2}{f(f_1 + f_2)}\right) \ , \tag{82}$$

where

$$K \equiv (2\pi R_{D1} C_{DF})^{-1} = 81,895 \text{ Hz} \ , \tag{83}$$

and

$$f_1 \equiv (2\pi R_{D1} C_{D1})^{-1} = 203.5 \text{ Hz} \quad , \quad f_2 \equiv (2\pi R_{DF} C_{DF})^{-1} = 408.6 \text{ Hz} \ . \tag{84}$$

It is plotted in Figure 45.

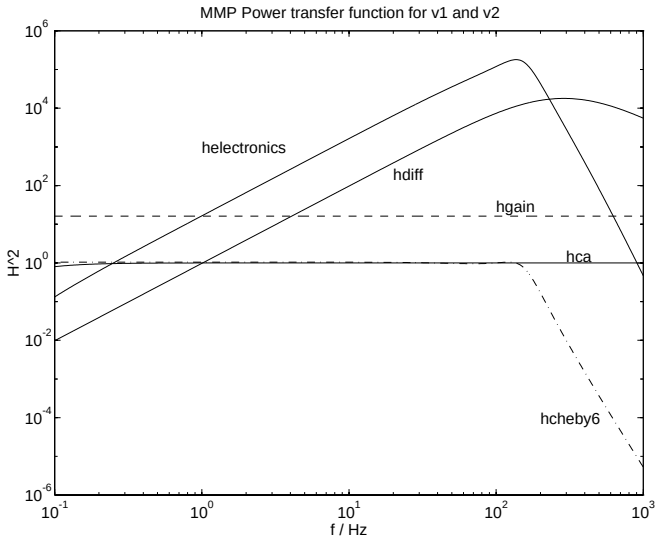

Figure 45: Power transfer functions for v1 and v2 electronics.

The third stage sets the gain with

$$H^2_{\text{gain}}(f) = \left(1 + \frac{R_{GF}}{R_{G1}}\right)^2 = 16.74 \quad , \quad \phi_{\text{gain}}(f) = 0 \ . \tag{85}$$

A 6-pole low-pass type 1 Tchebyscheff filter attentuates signals to minimize aliasing. The magnitude-squared response is given by (13).

The net electronic transfer function is the product of the separate components

$$H^2_{\text{electronics}}(f, C_S) = H^2_{\text{ca}}(f, C_S)\, H^2_{\text{diff}}(f)\, H^2_{\text{gain}} \tag{86}$$

$$\phi_{\text{electronics}}(f) = \phi_{\text{hca}} + \phi_{\text{hdiff}} \tag{87}$$

It is plotted in Figure 45.

The total transfer function is

$$H^2_{\text{total}}(f, S_v, C_S, w, f_c) = \left(\frac{wS_v}{2g}\right)^2 H^2_{\text{electronics}}(f) H^2_{\text{Oakey}}(f, w) H^2_{\text{Tch}}(f, f_c) \quad [\text{volts}^2\ (\text{m/s})^{-2}] \ . \tag{88}$$

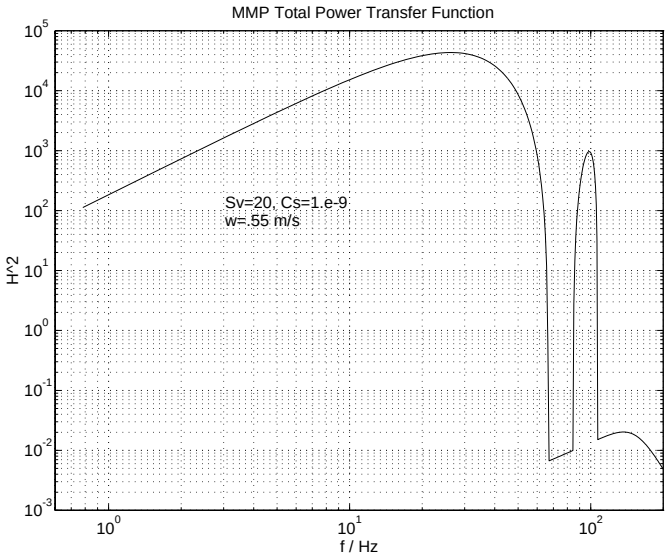

Figure 46: Total system power transfer function. Spectrum of raw v1 or v2 record in volts is divided by this to form a velocity spectrum in $\mathrm{m}^2\ \mathrm{s}^{-1}\ \mathrm{Hz}^{-1}$.

The scaling factor, $(wS_v/2g)^2$, comes from (76) and is about 0.58 for typical values of $S_v = 25$, $C_s = 1,000$ pF, and $w = 0.6$ m s^{-1}. It is shown in Figure 46.

Before 30 Jan 1995, the Tchebyscheff anti-alias filter had $f_c = 150$ Hz. On that day f_c was changed to 100 Hz. Spectra of raw data in volts^2 Hz^{-1} are divided by H^2_{total} to obtain velocity spectra in $\mathrm{m}^2\ \mathrm{s}^{-1}\ \mathrm{Hz}^{-1}$.

16.3 Data Conversion

16.3.1 Spectra

The power spectrum of recorded signals, converted to volts, is

$$\Phi_{\mathrm{R}}(f) = \frac{\Phi_u(k_3)}{w} H^2_{\mathrm{electronics}}(f, C_S) H^2_{\mathrm{Tch}}(f, f_c) H^2_{\mathrm{Oakey}}(f, w) \left(\frac{S_v w}{2g}\right)^2 \quad \left[\mathrm{V}^2\ \mathrm{Hz}^{-1}\right] . \tag{89}$$

Inverting gives the oceanic velocity spectrum,

$$\Phi_u(k_3) = \frac{w\Phi_{\mathrm{R}}(f)}{H^2_{\mathrm{electronics}}(f, C_S) H^2_{\mathrm{Tch}}(f, f_c) H^2_{\mathrm{Oakey}}(f, w)} \tag{90}$$

The spectrum of vertical shear is

$$\Phi_{\partial u/\partial z}(k_3) = (2\pi k_3)^2 \Phi_u(k_3) \quad \left[\mathrm{s}^{-2}\ \mathrm{cpm}^{-1}\right] . \tag{91}$$

The rate of viscous dissipation of turbulent kinetic energy, ϵ, is obtained by integrating the shear spectrum

$$\epsilon = 7.5\nu(s,T,P)\int_{k_0}^{k_u} \Phi_{\partial u/\partial z}(k_3)\, dk_3 \quad [\mathrm{W\,kg^{-1}}] \;, \tag{92}$$

where $\nu(s,T,P)$ is the kinematic viscosity, and k_0 and k_u are the lower and upper cutoffs determined by record length and the character of the data, respectively. Variations in ν are large enough that it should be evaluated at in-situ conditions.

The dissipation spectrum,

$$\phi_{\mathrm{diss}} = k_3 \Phi_{\partial u/\partial z}(k_3) \quad [\mathrm{s^{-2}}] \;, \tag{93}$$

shows the relative contributions of different wavenumbers to ϵ if plotted with a logarithmic k_3 axis and a linear abscissa.

16.4 Observed Characteristics

The spectrum of vertical shear from MMP3 is shown in figure 47.

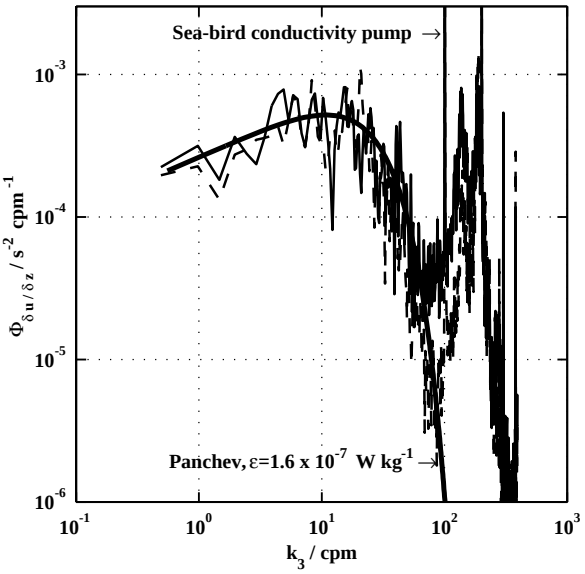

Figure 47: Airfoil shear spectrum, $\Phi_{\delta u/\delta z}(k_3$ from drop 7655 (taken in Puget Sound), from 145-165 m. Both probes are plotted, and the Panchev spectrum for $\epsilon = 1.6x10^{-7}Wkg^{-1}$ is plotted for reference.

17 Relative Velocity, vac1 and vac2

17.1 Sensor Description

MMP3 uses a 2-axis Neil Brown Instrument Systems Acoustic Current Meter (ACM) to measure relative velocity. The ACM electronics are housed in the upper main section of MMP3 (just below the flooded tail section) while the acoustic transducers are located near the ends of the four guard rods. The ACM measures the relative flow along the 0.15-m path between each pair of transducers. The x1 - x2 pair (vac1 channel) is parallel to the sensitive axis of accelerometers a1 and a3. The y1 - y2 pair (vac2 channel) is parallel to the sensitive axis of accelerometers a2 and a4. The vac1 and vac2 channels are sampled at 50 Hz and digitized with 16 bits. The anti-alias filters are 4-pole Tchebyschev filters with a 10 Hz cutoff frequency. Because of MMP3's motion the ACM measures a velocity different than that of the water. The ability to determine water velocity is dependent on the success of an instrument response model that corrects for tilt and MMP3's gross motion (section 19).

The ACM uses an acoustic differential travel time method of sensing currents. High frequency sound (2.75 MHz) is transmitted simultaneously and repetitively (5.333 kHz) between pairs of acoustic transducers to produce continuous wave bursts travelling in opposite directions. After the bursts are transmitted, each transducer is simultaneously connected to receiving circuitry that compares the phase of the arriving signals. The phase difference is directly proportional to the water velocity component parallel to the axis of a transducer pair. For example, when a continuous wave burst is transmitted at x1 and travels to x2 a burst is similarly transmitted at x2 and received at x1. In the presence of a current, the signal traveling with the current will be advanced in phase and the signal traveling against the current will be retarded in phase. The result is that the relative phase between the bursts received at x1 and x2 will depend on the acoustic frequency, spacing between x1 and x2, the speed of sound and the water velocity. To detect a 1 cm s^{-1}current, a direct measurement of the phase at the 2.75 MHz acoustic frequency would require time discrimination of less than 100 picoseconds. Instead the signals at x1 and x2 (y1 and y2) are heterodyned at 2.75 MHz + 157 Hz. The 157 Hz difference frequency resulting from the mixing process contains the phase information of the original 2.75 MHz acoustic signal. The time discrimination at this frequency is nearly 18,000 times less stringent.

The acoustic transducers are made of piezoelectric material 2PZT-5 in the form of a small disk, 4.45 mm in diameter and 0.76 mm thick. The piezoelectric elements are purchased from Staveley Sensors, East Hartford, CT. Each element is potted in a stainless steel tube with a hole through it for the transducer (open on each side). The tube is mounted inside a guard rod and positioned near the center of an opening larger than the transducer face. Placing a metal rod through a 3.2-mm hole in the end each guard rod aligns the transducers. Twisted-pair magnet wire connects each transducer assembly to a bulkhead connector in the upper end cap.

17.2 Data Conversion

Each velocity component vac is given by

$$\text{vac}[\text{cm s}^{-1}] = \frac{0.025\text{VKC}^2}{\text{fd}} \tag{94}$$

where,
V = output voltage from velocity module in volts
C = speed of sound in water in cm/sec
K = calibration factor = 0.94
d = transducer spacing = 15 cm
f = acoustic frequency = 2,750,497 Hz The sensitivity is 78 $\text{Vcm}^{-1}\text{sec}^{-1}$. The full range (limited by the A/D converter ± 5V input range) is ± 64.1 cm s^{-1}.

The speed of sound required to calculate the water current velocities is given by

$$\text{C}/100 = 1449 + 4.6\text{T} - 0.055\text{T}^2 + 0.0003\text{T}^3 + (1.39 - 0.012\text{T})(\text{S} - 35) + 0.017\text{D} \tag{95}$$

where,
C = speed of sound in water in cm/sec
T = temperature in degrees Celsius
S = salinity in parts per thousand
D = depth below surface in meters

17.3 Observed Characteristics

Please refer to section 19 for sample acm data.

18 Heading, hdg

18.1 Sensor Description

To determine heading MMP3 uses a Model C100 Compass Engine made by KVH Industries, 110 Enterprise Center, Middletown, RI 02842. The C100 electronic compass consists of a detachable toroidal fluxgate sensing element (SE-25 coil), a small electronics board, and menu-driven software which allows specific parameters of individual outputs to be controlled via a RS232 input. The standard SE-25 coil is mounted in a level attitude within MMP3 with the "FORWARD" arrow pointing to the ACM y2 transducer; i.e., parallel to the y-axis. This sensor will operate through tilt ranges of $\pm 16^{\circ}$. The compass has an accuracy of $\pm 0.5^{\circ}$, repeatability of $\pm 0.2^{\circ}$and resolution of $\pm 0.1^{\circ}$. It is configured to output synchronous data from the digital port in a strobed mode. The compass is strobed every 120 ms. No damping is applied.

The compass is configured and calibrated by running a pc program C100USR.EXE. The pc is connected via RS232 and a 3-pin Impulse connector near the middle of MMP3's main pressure case. The Circular Autocompensation Procedure is performed by slowly rotating the instrument in a circle (1 to 2 minutes for a complete rotation).

18.2 Data Conversion

The C100 electronic compass outputs a 16-bit binary word. The data is msbit first with a range of 0 to 3599 corresponding to the magnetic heading in tenths of degree; i.e.,

$$\text{MagneticHeading[degrees]} = 0.1(\text{hdg}) \tag{96}$$

Heading data is updated every third scan for a sample rate of 8.33 Hz.

18.3 Observed Characteristics

A typical heading plot is shown in figure 48.

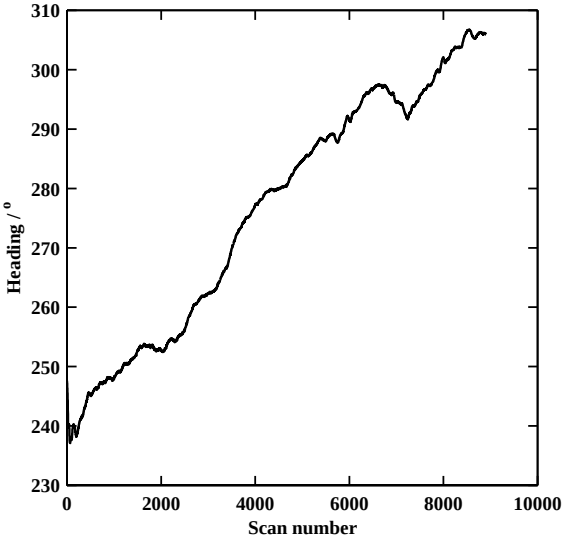

Figure 48: A typical heading record.

19 Modeling of MMP3 Motion

19.1 Introduction

As discussed in section 17, the acoustic current meter measures the velocity relative to MMP3. Following *Winkel et al.* (1994), this velocity is used to construct profiles of ocean velocity, relative to a depth-independent constant. Two types of reference frame issues cause these measurements to differ from the earth-frame water velocity. First, MMP's tilt and swinging contaminate the perceived velocity. These effects can be removed to a large degree using tilt estimated from the accelerometers (section 8), providing estimates of instrument-relative horizontal velocity. The second reference-frame transformation involves accounting for MMP's horizontal motion as it falls. These two corrections are discussed next, and then results are shown. The use of the LXT tracking system to diagnose the success of the method is described last.

19.2 Tilt and Swinging

The acceleration data are used to compute tilts as in section 8. The tilt data are then used to correct the raw ACM signal for tilt and swinging, according to

$$v_{acm}(t) = v_{rel}(t) - W(t)\theta(t) - L_v \partial/\partial t \theta(t). \tag{97}$$

W(t) is the instantaneous fall speed, L_v is the distance from the center of effective mass to the ACM, and θ is measured counterclockwise. The raw velocity, tilt and swinging terms, and the corrected signal are plotted for a typical profile in figure 49, with a reduced depth range shown to the right. Except for near the surface, these corrections are usually small compared with the measured signal (but noticeable, unlike for the much larger MSP).

Spectra computed from the region plotted to the right in figure 49 are shown in figure 50. For this region, the corrections are quite small. This is generally true below the upper 10-20 m.

The heading (hdg, section 18) is then used to transform the relative velocities into earth coordinates.

19.3 Point-mass model

Once tilt and swinging are removed, we have profiles of MMP-relative horizontal velocity. These differ from ocean velocity:

$$\mathbf{u_{rel}} = \mathbf{u_{wat}} - \mathbf{u_{MMP}}. \tag{98}$$

$\mathbf{u_{wat}}$ is the true ocean velocity, and $\mathbf{u_{MMP}}$ is the horizontal velocity of the center of mass of the package. Accurate determination of $\mathbf{u_{wat}}$ requires knowledge of $\mathbf{u_{MMP}}$, which must be modeled. The same point-mass model used by *Winkel et al.* (1994) was used with good results.

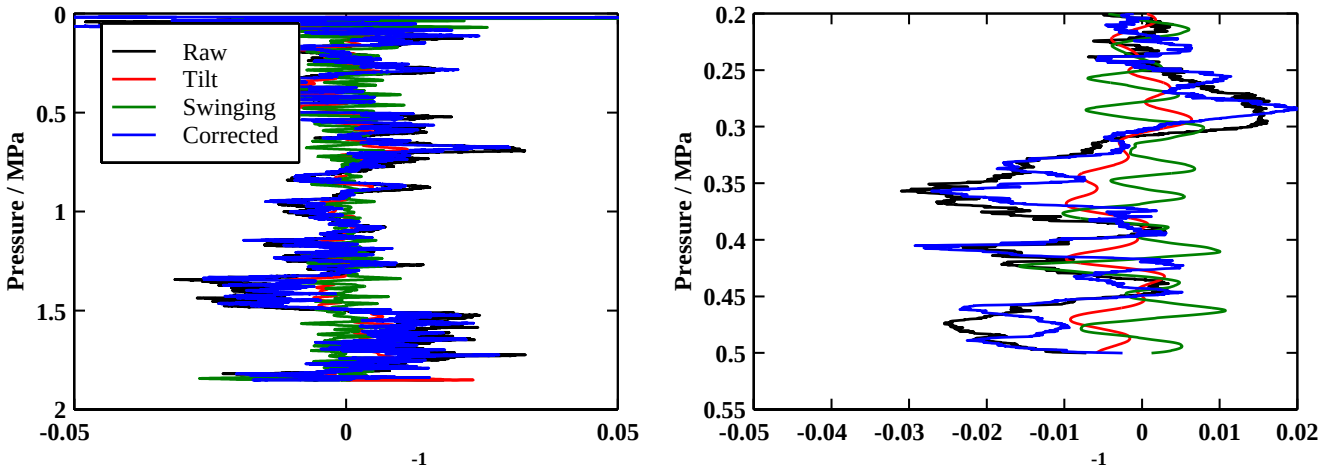

Figure 49: Typical raw (black) and corrected velocities from 0-200 m (left) and 110-150 m (right) in profile WHICH, taken in Puget Sound during August 1999. The corrected profiles have tilt (red) and swinging (green) terms removed.

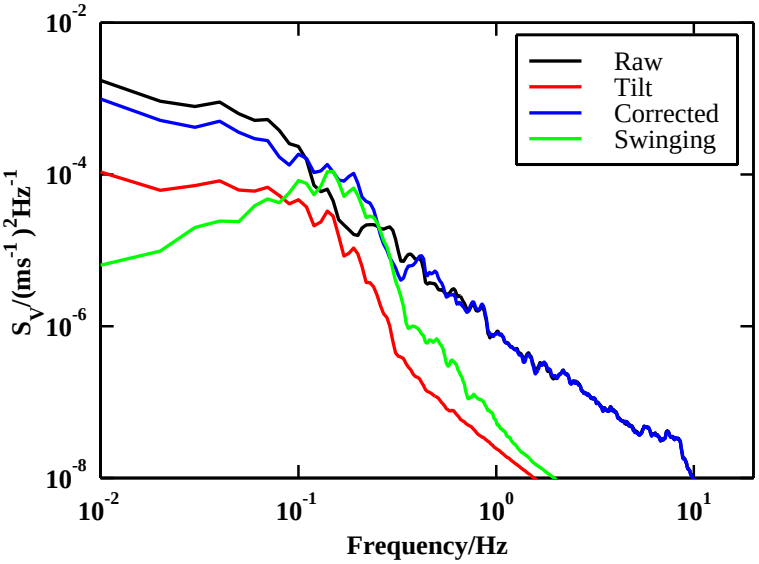

Figure 50: Spectra of typical raw (black) and corrected (blue) acm data. The spectra of the tilt (red) and swinging (green) terms are also shown.

The parameters used are shown in 19.3. All parameters are quite close to physical values, with the exception of Bf. The tilt correction was decreased nearly a factor of two to remove a slight valley near 0.2 cpm.

The offsets in the acm and accelerometers are removed for each profile. As a result, information about the very largest scales is lost. We must address these offsets if we are to

Parameter	Description	Value	Physical Value
r_N [m]	Radius	0.10	0.07
r_T [m]	Radius	0.25	0.26
Z_N [m]	Distance to nose	0.4	0.46
Z_T [m]	Distance to tail	1.3	1.22
D_N [m]	Nose Window	0.3	0.3
D_T [m]	Tail Window	0.5	0.5
L_v [m]	Distance from CM to ACM	1.1	1.1
L_a [m]	Distance from CM to a1	1.1	1.1
B_f []	Tilt Parameter	0.6	1.0
$\beta_o[s^{-2}]$	Righting	1.1	1?
$\beta_1[S^{-1}]$	Damping	1.1	1?
$I_e[kg\ m^2]$	Moment of Inertia	12	12
M_{wet} [kg]	Wet Mass (incl. enclosed water)	34.73	34.73
M_{eff} [kg]	Effective Mass (incl. added mass)	66.18	66.18

Table 12: Model parameters used for MMP3 force model, and "physical" parameters estimated from Gordy Welsh's drawings and specifications.

resolve the largest scales. On the other hand, these will usually be able to be matched to an ADCP in practice.

19.4 Model Velocity profiles

Sample model profiles of u and v taken during the HOME survey leg are compared to an XCP drop taken about 20 minutes before) in figure 51. The depths of the XCP velocities were matched to MMP's using the temperature profiles. The model and XCP velocity profiles generally agree; however, notice the largest scales is poor due to the removal of mean relative velocity and tilt.

19.5 Shear Spectra

To demonstrate the degree to which the motion-corrected ACM data can be used to determine shear spectra, composite shear wavenumber spectra are formed by meshing XCP (<0.1 cpm), motion-corrected ACM (0.01-5 cpm) and shear probe (>1 cpm) data. In each case, each of the 3 profiles of velocity from 80-300 m was demeaned, detrended and hanned. (In the case of the XCP, only one profile was available). The velocity spectrum was computed using an 80-m window, yielding about 9 degrees of freedom. The shear spectrum was computed using $\Phi_{shear} = (2\pi k)^2 \Phi vel$ and plotted in figure 52. The spectra of raw acm shear, before and after the tilt/swinging corrections, are shown in light green/blue.

In the range 0.01-0.1 cpm, the XCP spectrum is in fair agreement with that from the

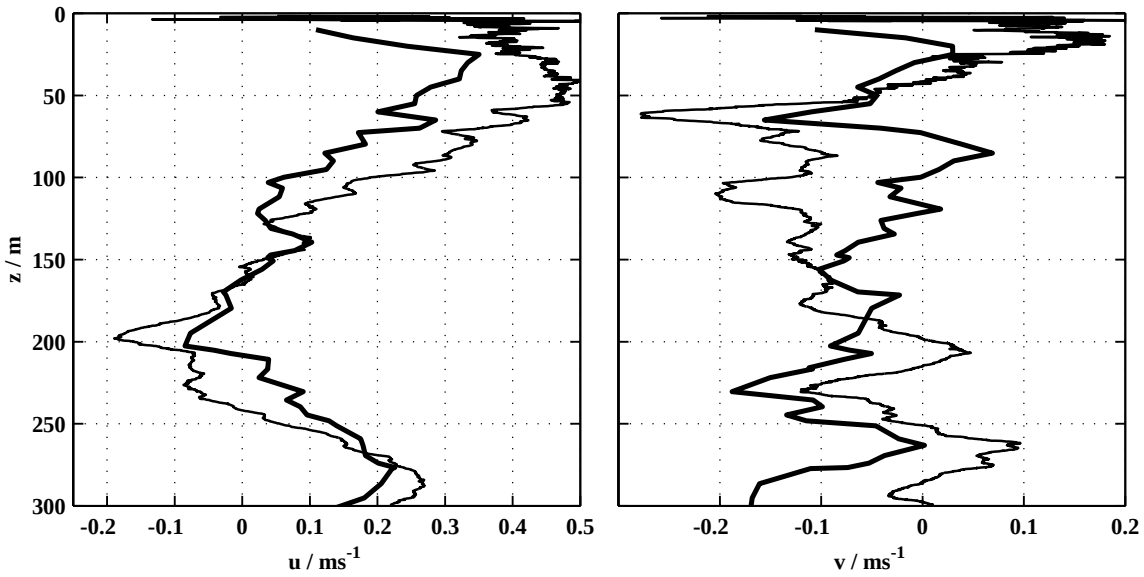

Figure 51: Comparison between motion-corrected ACM velocity for MMP11444 (thin) and an XCP drop taken 20 minutes previously during HOME's survey leg.

motion-corrected ACM records (heavy blue). For k > 0.1 cpm, the ACM spectrum falls off as approximately k^{-1}, in decent agreement with the GM76 canonical spectrum (black dotted line).

Airfoil spectra (magenta) are formed by averaging over all depths, as in the ACM and XCP spectra, ignoring concerns of nonstationarity. The Panchev spectrum corresponding to the depth-mean dissipation rate of $\overline{\epsilon} = 4 \times 10^{-9}$W kg^{-1} is overplotted.

The ACM spectra blend smoothly in near 1 cpm with the airfoil spectra. Agreement is seen up until about 4-5 cpm, when the noise on the vacy channel causes the acm spectra to rise higher.

19.6 Acoustic Tracking

A Trackpoint LXT ultra-short-baseline tracking system yields estimates of range, azimuth and elevation angles of the vehicle. The range precision is well under a meter; however, uncertainties in angle degrade the absolute precision to several meters. Since this results in large velocity uncertainty, the tracking is not useful for determining velocity (much less shear). However, the system is useful as a check on the model output. These data are collected continuously in time and logged with Steve's LXTLOG program. The MMP3 drop start times can be used to map the LXT time series onto particular drops.

The LXT returns the position of MMP3 relative to the ship. The bottom tracking velocity is integrated to determine the ship's position. (Better yet, differential GPS could be employed.) Together with ship heading information, it is possible to determine the absolute position of the ship and MMP3 in earth coordinates.

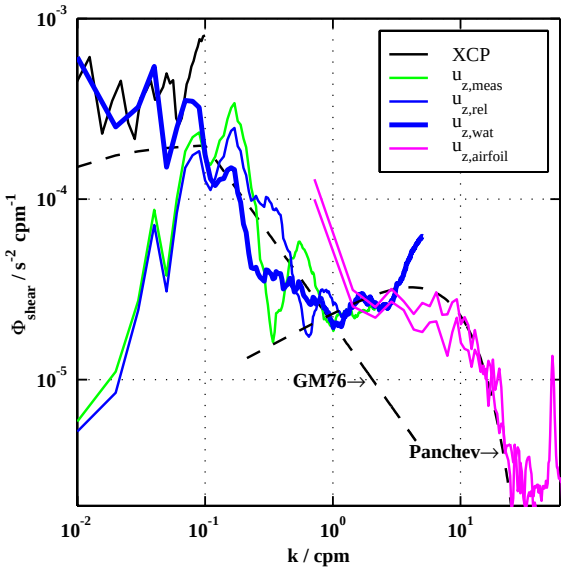

Figure 52: Wavenumber spectra of zonal shear from an XCP drop (black), pre-model ACM (light green/blue), motion-corrected ACM (heavy blue), and the two shear probes (black). Individual spectra from 11 profiles are plotted as dots, and their mean with heavy lines (red and blue are the two airfoils). The ADCP and ACM noise spectra are shown with black and green dotted lines, respectively. The dotted black line to the right is the Panchev spectrum for $\overline{\epsilon} = 4 \times 10^{-9}$W kg^{-1}.

A sample track determined from the tracking system is shown in green in figure 53. The integrated water velocity, or the position of water parcels at the depth of MMP3, is plotted in blue.

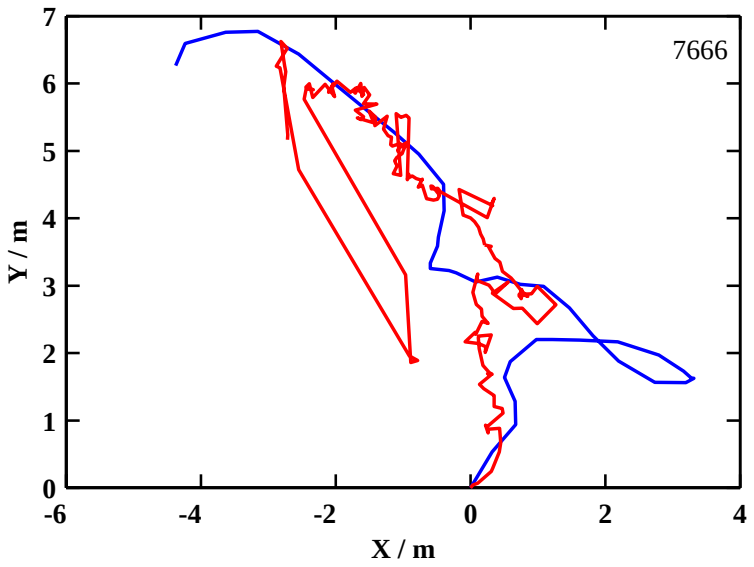

Figure 53: A typical vehicle track (red), from LXT tracking, and water track (blue). The large southward displacement near the end of the drop is a glitch resulting from a bad angle return.

BIBLIOGRAPHY

References

Bennett, R. S., The calibration of thermistors over the temperature range 0°C to 30°C, *Deep-Sea Res.*, *19*, 157–163, 1972.

Gregg, M., and T. Meagher, The dynamic response of glass rod thermistors, *J. Geophys. Res.*, *85*, 2779–2786, 1980.

Gregg, M., T. Meagher, A. Pederson, and E. Aagaard, Low noise temperature microstructure measurements with thermistors, *Deep-Sea Res.*, *25*, 843–856, 1978.

Irish, J. D., and M. D. Levine, Digitizing error from period and frequency counting techniques, *Deep-Sea Res.*, *25*, 211–219, 1978.

Ninnis, R., *The effects of spatial averaging on air-foil probe measurements of oceanic velocity microstructure*, Ph.D. thesis, Univ. of British Columbia, Vancouver, Canada, 1984.

Oakey, N. S., An instrument to measure oceanic turbulence and microstructure, Rept. Series BI-R-77-3, Bedford Inst. Oceanogr., Dartmouth, N.S., Canada, 1977.

Osborn, T. R., and W. R. Crawford, An airfoil probe for measuring turbulent velocity fluctuations in water, in *Air-Sea Interactions: Instruments and Methods*, edited by F. Dobson, L. Hasse, and R. Davis, 369–386, Plenum, New York, 1980.

Otnes, R. K., and L. Enochson, *Applied Time Series Analysis, Vol. 1: Basic Techniques*, Wiley, New York, N. Y., 1978.

Payne, R. E., and W. Smith, Spectra of frequency counting digitization errors, *Deep-Sea Res.*, 1980.

Pederson, A., and M. Gregg, Development of a small *in-situ* conductivity instrument, *IEEE J. Ocean Engr.*, *OE-4*, 69–75, 1979.

Schmitt, R. W., J. M. Toole, and R. L. Koehler, The development of a fine- and microstructure profiler, *J. Atmos. Ocean. Tech.*, *5*, 484–500, 1988.

Williams, A. B., *Electronic Filter Design Handbook*, McGraw-Hill, New York, 1981.

Winkel, D. P., M. C. Gregg, B. Bell, and T. Sanford, Resolving velocity profiles with the Multi-scale Profiler, *APL Technical Report*, *TR9414*, 1–45, 1994.